Ultrasonic velocity measurements in liquids with high resolution—techniques, selected applications and perspectives

2008 Meas. Sci. Technol. 19 062001

(http://iopscience.iop.org/0957-0233/19/6/062001)

Meas. Sci. Technol. **19** (2008) 062001 (21pp) doi:10.1088/0957-0233/19/6/062001

TOPICAL REVIEW

Ultrasonic velocity measurements in liquids with high resolution—techniques, selected applications and perspectives

Udo Kaatze[1], **Frieder Eggers**[2] **and Karl Lautscham**[1]

[1] Drittes Physikalisches Institut, Georg August Universität, Friedrich-Hund-Platz 1, 37077 Göttingen, Germany
[2] Retired, formerly at Max-Planck-Institut für Biophysikalische Chemie, Am Faßberg 11, 37077 Göttingen, Germany

Received 20 November 2007, in final form 8 January 2008
Published 29 April 2008
Online at stacks.iop.org/MST/19/062001

Abstract
This review gives a short introduction into the principles of sound velocity measurements. The fundamentals of acoustical methods using continuous waves, pulse modulated signals and sharp pulses are summarized. Methods employing optical wave interactions with continuous ultrasonic waves are also described briefly. Recent advances in the different methods are presented, and the technical status of the currently preferred techniques is discussed in view of their merits and limitations, too. Particular emphasis is given to the sensitivity and accuracy of the methods. Selected examples of measurement applications indicate the extended usability spectrum in basic research as well as in materials' characterization, manufacturing processes and control routines.

Keywords: sound velocity, adiabatic compressibility, ultrasonic spectrometry, resonator techniques, pulse methods

1. Introduction

A characteristic parameter of matter, particularly liquids, is its specific volume V, which reflects, in an obvious way, interparticle forces and particle packing. Direct access to molecular interactions and structure can be obtained from the isothermal compressibility

$$\kappa_T = -\frac{1}{V}\left(\frac{\partial V}{\partial p}\right)_T = -\left(\frac{\partial \ln V}{\partial p}\right)_T \tag{1}$$

(p: pressure), which is a fundamental property in many fields of science. Direct methods for measuring liquid κ_T, however, are either relatively inaccurate or laborious and are, therefore, less appropriate for many applications. For this reason, more interest is directed towards the isentropic compressibility:

$$\kappa_S = -\frac{1}{V}\left(\frac{\partial V}{\partial p}\right)_S = -\left(\frac{\partial \ln V}{\partial p}\right)_S \tag{2}$$

from which κ_T can be calculated, using well-known thermodynamic relations [1, 2]. According to the Newton–Laplace equation

$$\kappa_S = \frac{1}{\rho_M c_M^2}, \tag{3}$$

the isentropic (adiabatic) compressiblity κ_S is usually determined from the density ρ_M and the sound velocity c_M of the liquid medium. Whereas precise densitometers have existed for many years, allowing measurements with small sample volumes and relative errors below 10^{-6} [3], many efforts have been made in recent years to develop easy-to-handle, especially automatic, sound velocimeters of comparable accuracy [4–11]. Due to the obtained measurement quality, pushing the resolution of current ultrasonic velocimeters to 10^{-7}, such measurements are used more and more often, not only for fundamental studies in physical chemistry [12–18], biophysics and biochemistry [19–35], but also for numerous technical applications, e.g.

in chemical engineering. Examples are to be found in the preparation and production of colloids and emulsions [36–45], in the pharmaceutical industry [46–51] and in the processing of foods and beverages [52–69].

A major advantage of sound velocity methods is that nearly all chemical reactions exhibit a dependence of their equilibrium constant upon pressure and/or temperature, and therefore couple to the acoustical field; in addition, sonic studies do not require extra (artificial) molecular labels or markers, which can often disturb the native system under study [70–75]. As each reaction is associated with a characteristic time constant τ, a frequency-dependent sound velocity measurement (velocity spectrometry) can indicate a relaxation process and can thus permit the determination of τ, which will be named relaxation time further on. If the angular frequency $\omega = 2\pi\nu$ (ν: frequency) of a harmonically oscillating acoustic field approaches the relaxation rate τ^{-1}, fewer and fewer particles are able to follow the perturbing parameter. Thereby, the liquid compressibility κ_S decreases with frequency; in consequence the sound velocity increases, exhibiting characteristic dispersion effects [76–79]. Because of relaxation in the reaction (with the time constant τ), a phase lag between the pressure and the density oscillations in the molecular system, initiated by the sound wave, results, which causes a conversion of sonic energy into heat, mainly from viscous effects. Sound velocity dispersion due to relaxation is associated with absorption. Under usual conditions, with the relaxing imaginary part of the (complex) compressibility being small as compared to the nonrelaxing real one, a propagating acoustical plane wave decays exponentially, with a frequency-dependent absorption coefficient α_M, which, for a single relaxation process with relaxation time τ, is described by [80, 81]

$$\alpha_M = B'\omega^2 + \frac{A\omega^2\tau}{1+(\omega\tau)^2}, \tag{4}$$

whereas the sound velocity $c_M(\omega)$ follows the relation

$$\frac{1}{c_M(\omega)} = \frac{1}{c_M(\infty)} + \frac{A}{1+(\omega\tau)^2}. \tag{5}$$

The term $B'\omega^2$ represents the asymptotic high frequency part in the absorption coefficient, A is an amplitude and $c_M(\infty)$ is the sound velocity at frequencies far above the relaxation region. As we are not interested in the asymptotic high frequency absorption term, equation (4) may be rewritten to yield the excess absorption per wavelength:

$$(\alpha_M\lambda)_{\text{exc}} = \alpha_M\lambda - B\nu = 2\pi c_M \frac{A\omega\tau}{1+(\omega\tau)^2}, \tag{6}$$

where $\lambda = c_M/\nu$ and $B = 4\pi^2 c_M B'$. From equation (5) follows

$$c_M(\omega) = c_M(\infty)\cdot\left[1 - c_M(\infty)\frac{A}{1+(\omega\tau)^2 + c_M(\infty)A}\right]. \tag{7}$$

In figure 1, as an example, experimental sound velocity values of an aqueous solution, together with corresponding excess absorption per wavelength data, are displayed as a function of frequency [81]. Equations (6) and (7) demonstrate that both quantities are correlated, in accordance with the Kramers–Kronig equations [82, 83]. Hence, both

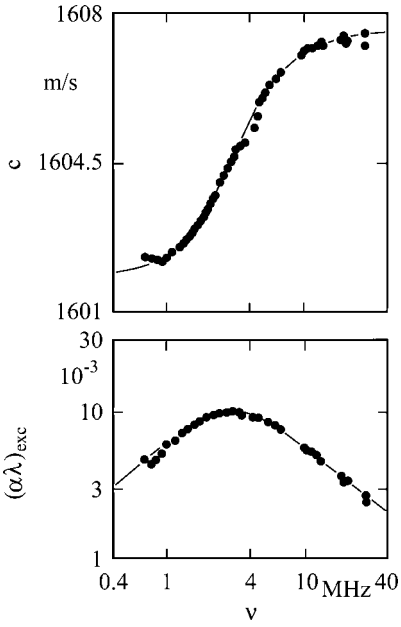

Figure 1. Sound velocity c and excess absorption per wavelength $(\alpha\lambda)_{\text{exc}}$ as a function of frequency ν for a solution of 1 mol l^{-1} imidazol, 0.5 mol l^{-1} maleic acid and 1 mol l^{-1} sodium hydroxide in water at 40 °C [81].

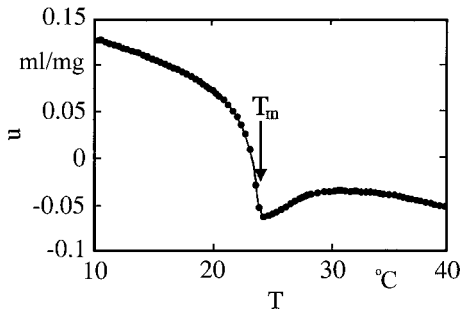

Figure 2. Sound velocity number $u = (c - c_0)/(c_0\hat{C})$ of a vesicle solution of 1,4-dimyristoyl-L-3-phosphatidylcholin in water versus temperature T [84]; c_0: solvent sound velocity, $\hat{C} = 5$ mg ml^{-1}: solute concentration.

(a) sound velocity spectrometry and (b) sound absorption spectrometry are suitable for a nondestructive and reversible, 'non-contaminating' investigation of fast chemical reactions, including biomolecular ones, and for a determination of rate constants, which may be difficult to obtain otherwise.

Frequently, sound velocity measurements do not aim at the investigation of relaxation phenomena, but utilize the high sensitivity of sonic velocimetry with respect to structural changes in the sample. In figure 2, the sound velocity temperature profile of a phopholipid bilayer vesicle suspension is shown near the main transition, where the membrane passes from a gel phase to a fluid phase [84]. In the former phase the arrangement of phospholipid molecules displays a high degree of order, with the hydocarbon chains almost completely stretched. In the latter the chains are molten and, by analogy with liquid alkanes, exhibit a noticeable concentration of structural isomers. The compressibility of the membrane increases at such phase transition, associated

with a sound velocity decrease. As the volume fluctuations, reflected by the compressibility, and the enthalpy fluctuations of the phospholipid molecules are proportional to each other, sound velocity and heat capacity temperature profiles are related to each other [22, 28]. Therefore, sound velocity measurements permit a reliable determination of the phase transition temperature and also give a deeper insight into the correlation of mechanical properties of membrane systems in terms of thermal properties and vice versa [85].

In basic research sound velocity measurements are increasingly used; in addition, they are often employed in the process control of manufacturing procedures and also in a routine monitoring of quality changes of complex (viscoelastic) products during and after manufacture. Because of its outstanding sensitivity to liquid states, sound velocity is a favourable parameter for such applications. Sound velocity measurements can be quickly performed and permit an examination of optically opaque samples.

In this review several methods of sound velocity measurements, matched to the widespread applications, will be reviewed briefly. General information about acoustics, especially sound fields, transducers and applied techniques, has already been presented in numerous monographs [4, 71, 72, 74, 76–78, 86–94], book contributions [70, 73, 79, 95–97] and reviews [5, 75, 98, 99]. Early benchmark publications are referred to, for instance, in [70, 76, 78, 86, 87, 95].

2. Principles of methods

2.1. Phase velocity and group velocity

The sound velocity in the Newton–Laplace equation (3) is the phase velocity of a wave, i.e. the velocity at which the phase of any single-frequency component of the sonic signal is propagating. With the angular frequency ω and the wave number k, the phase velocity is

$$c = \omega/k. \tag{8}$$

A simple way for measuring c is to determine the wavelength $\lambda = 2\pi/k$ of a single-frequency plane wave at frequency $\nu = \omega/2\pi$. Other methods in use obtain the sound velocity from the time interval Δt, which a 'sharp' pulse needs to propagate through a distance Δx. This time is controlled by the group velocity

$$c_g = \mathrm{d}\omega/\mathrm{d}k, \tag{9}$$

i.e. the propagation velocity for amplitude-modulated signals. According to equation (8)

$$\mathrm{d}\omega = c\,\mathrm{d}k + k\,\mathrm{d}c, \tag{10}$$

and thus

$$c_g = c + k\,\mathrm{d}c/\mathrm{d}k \tag{11}$$

as well as

$$\frac{1}{c_g} = \frac{1}{c} + \frac{\nu}{c^2}\frac{\mathrm{d}c}{\mathrm{d}\nu}. \tag{12}$$

The group velocity c_g of a medium equals the phase velocity c only with no dispersion in c, i.e. for $\mathrm{d}c/\mathrm{d}\nu = 0$. For liquids with relaxation behaviour, characterized e.g. by equation (5), c_g differs from c. This difference is shown in figure 3 for the frequency-dependent velocity in a 0.4 mol l^{-1} zinc chloride aqueous solution; at 10 MHz, $k \times \mathrm{d}c/\mathrm{d}k = 7$ m s^{-1} or $(c_g - c)/c = 4.6 \times 10^{-3}$. For a solution of imidazol, malic acid and sodium hydroxide in water at 4 MHz (figure 1), $(c_g - c)/c = 1.9 \times 10^{-3}$. Such differences between group and phase velocities, exceeding the experimental error of current velocimeters, are clearly detectable; therefore, they should be included in quantitative evaluations of group velocity data.

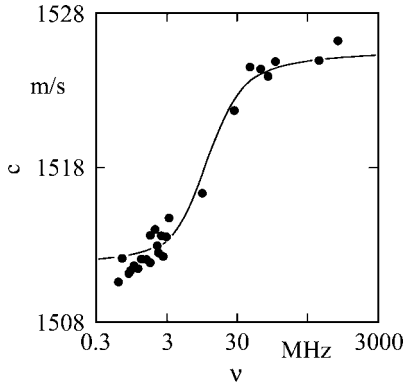

Figure 3. Velocity spectrum of an aqueous 0.4 mol l^{-1} zinc chloride solution at 25 °C [100]. Data obtained as a byproduct of ultrasonic absorption spectrometry with resonators at lower frequencies (0.5 MHz $\leqslant \nu \leqslant$ 10 MHz) and with pulse-modulated signal transmission techniques at higher frequencies (5 MHz $\leqslant \nu \leqslant$ 3000 MHz). ——: relaxation spectral function with parameters from corresponding absorption spectrum.

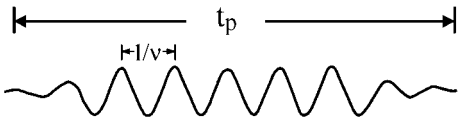

Figure 4. Waveform of a pulse-modulated sinusoidal signal.

2.2. Pulse methods

Pulse methods are among the most simple and widely used techniques for measuring liquid sound velocities. Many variations of pulse techniques have been described so far. With respect to signal shape and sample excitation, they can be subdivided into two categories as follows. The first comprises methods which utilize plane wave sound propagation at one well-defined frequency ν_0 [101–111]. Square-pulse modulated sinusoidal sound waves are used for the purpose of direct delay time measurements, in order to get a clear separation from multiply reflected signals and electromagnetic crosstalk by gating (figure 4). Due to the limited pulse duration time t_P, a wave segment in a rectangularly switched sinusoidal signal is not single-frequency. In addition to the carrier frequency there are side bands, resulting in an effective bandwidth [112]

$$\Delta\nu_P \approx 1/t_P. \tag{13}$$

Typical values for t_P are between 1 and 20 μs; for a carrier frequency ν_0 near 10 MHz [101], corresponding $\Delta\nu_P/\nu_0$

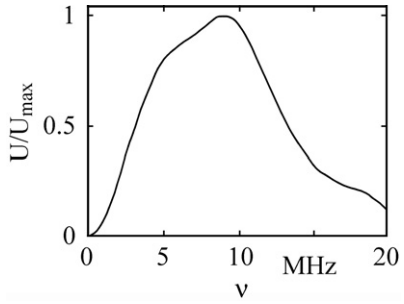

Figure 5. Amplitude spectrum of a broadband pulse. Relative voltage (maximum value U_{max}) versus frequency ν [117].

values are then between 0.005 and 0.1. This bandwidth has to be taken into account when the frequency dependence of sound velocity is the focus of interest. We will refer to this category of pulse measurements as 'narrow-band pulse techniques'. Likewise the method of determining directly the difference between the sound velocities in the sample and in a reference liquid [113, 114] uses nearly single-frequency signals. In order to measure the phase of the signal transmitted through the specimen cell, the output of the receiver transducer is added to a reference signal from the harmonic signal generator. Pulse-modulated signals are applied just to gate out multiply reflected waveforms. Despite the nonvanishing signal bandwidth $\Delta\nu_P$ (equation (13)), narrow-band pulse techniques are considered to yield the true phase velocity c. Sound velocities obtained as a byproduct from pulse-modulated attenuation measurements [115, 116] also belong to this group of data.

The other category employs sharp ($t_P \leqslant 1$ μs) pulses [42, 58, 69, 117–119] with a wider frequency spectrum (figure 5). As in common sonography in medicine, the usage of sharp pulses requires broadband transducer (mostly piezoelectric) systems. Conventional sound velocity measurements with sharp pulses are based on a precise determination of the time interval Δt required for signal passage through the medium over a distance Δx. If Δx is accurately known, the Δt measurement, in addition to its simplicity, offers high precision for sound velocity determination. From those sharp pulse measurements, the group velocity is obtained as

$$c_g = \Delta x/\Delta t. \tag{14}$$

Sharp pulse techniques are limited by an inherent finite frequency bandwidth (instead of a single frequency) associated with the c_g data.

Various methods for Δt determination by narrow-band and by sharp pulse measurements have been reported. We describe the principle of the convenient 'sing-around' method [101–103, 106, 108, 120, 121] in a simplified form, sketched in figure 6. The pulse-modulated signal or the sharp pulse from a signal generator (1) is converted by a piezoelectric transmitter (2a) in the specimen cell (2). The generated acoustic signal traverses the sample (2b), is detected by a piezoelectric receiver (2c) and is amplified in order to increase its flange steepness. The amplified signal triggers a monostable multivibrator (4), which generates a square pulse, incrementing a counter (5) and

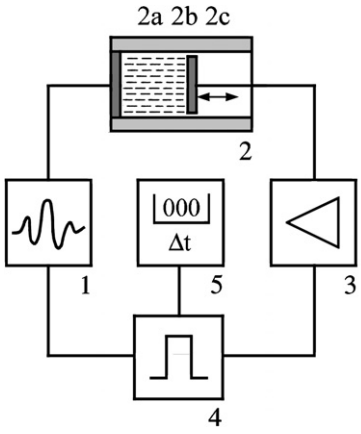

Figure 6. Block diagram of a basic sing-around measuring system. 1: signal generator, 2: specimen cell, 2a: transmitter crystal, 2b: liquid sample, 2c: receiver crystal, 3: amplifier, 4: square-pulse signal generator, 5: counter.

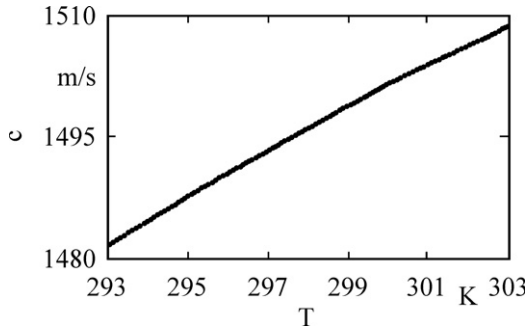

Figure 7. Sound velocity c in water versus temperature T (293 K $\leqslant$ $T \leqslant$ 303 K) [123].

triggering the signal generator (1) simultaneously. The total time delay

$$\Delta t_{tot} = \Delta t + t_e \tag{15}$$

between two subsequent signals is the sum of the time interval Δt in which a signal passes the sample distance Δx and a time delay t_e originating from the electronic system. The latter is either determined by calibration with a reference liquid of precisely known sound velocity or can be eliminated by a variation of the sonic pathlength (figure 6). For two pathlengths Δx_1 and Δx_2

$$c \text{ resp. } c_g = (\Delta x_1 - \Delta x_2)/(\Delta t_1 - \Delta t_2). \tag{16}$$

For velocity data from sing-around systems, a precision near 10^{-7} has been stated [120]. In order to achieve this accuracy, however, a high sample temperature stabilization is mandatory [122]; for example, in water at 25 °C (figure 7) a change of the sound velocity by 1 part in 10^7 or 0.15 mm s^{-1} corresponds to a temperature shift of only 50 μK [123].

Another frequently used method for velocity measurements employs pulses propagating through the sample and reflected back and forth as echoes [6, 9, 11, 42, 56, 104, 105, 109, 110, 124–126]. This reflection method needs only one transducer, active both as a transmitter and as a receiver, and a passive sound reflector. Pulse-echo methods

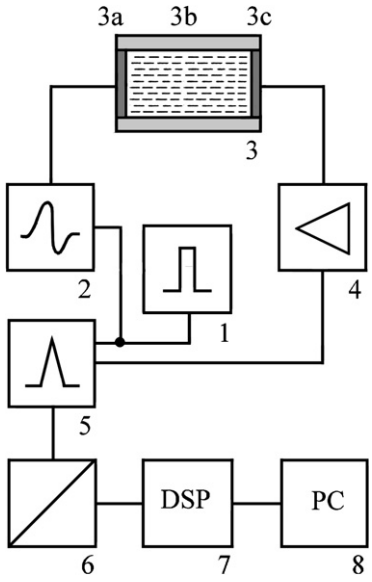

Figure 8. Block diagram for measurement of the phase spectrum of a sharp pulse. 1: trigger pulse generator, 2: pulse generator, 3: specimen cell, 3a and 3c: transducers, 3b: sample liquid, 4: broadband amplifier, 5: sampler, 6: D/A converter, 7: FFT and data processor board, 8: computer.

exist for narrow-band pulse-modulated signals as well as for sharp pulses. Delay time measurements obtained in this way agree with those from transmission techniques. Details of these methods will be discussed in section 3.

The broad frequency spectrum of sharp pulses (figure 5) allows us to determine group and phase velocities as well as the attenuation coefficient in a considerable frequency range [42, 58, 69, 117, 118, 127]. In this respect 'broadband-pulse' measurements resemble time domain methods, such as pressure and electrical field jump and, last but not least, temperature jump techniques [70, 74, 95, 99, 128, 129]. In the past and still today, these transient methods have been successfully applied for the study of fast chemical reactions. Basically, the response of the system after step-function excitation (temperature, pressure, electric field) is observed here.

The broadband pulse technique is based on a Fourier analysis of a primarily sharp pulse $u(x_i, t)$ after its interaction with the sample (x_i: interaction length). Both transmission and echo techniques can be combined with a fast Fourier transformation algorithm (figure 8), yielding the phase spectrum $\Phi(\omega)$ of $u(x_i, t)$ from which the dispersion relation

$$k = \hat{k}(\omega) \tag{17}$$

can be derived as [117]

$$\hat{k}(\omega) = [\Phi(\omega) - \Phi_0]/x_i, \tag{18}$$

with $\Phi_0 = \omega\xi_0$, where ξ_0 is a constant. According to equation (8), the phase velocity can be obtained from the dispersion relation

$$c(\omega) = \omega x_i[\Phi(\omega) - \Phi_0]^{-1} \tag{19}$$

and the group velocity is calculated from the derivative of the phase spectrum

$$c_g(\omega) = x_i[\mathrm{d}\Phi/\mathrm{d}\omega - \xi_0]^{-1}. \tag{20}$$

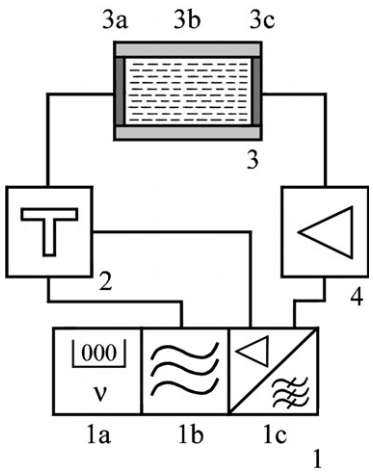

Figure 9. Block diagram for resonator transfer function measurements with a network analyser 1; components are 1a: RF synthesizer, 1b: signal generator, 1c: two-channel (sample and reference) superheterodyne receiver, 2: coaxial signal splitter, 3: specimen cell with 3a and 3c: transducers, 3b: sample liquid, 4: broadband preamplifier.

2.3. Continuous wave methods

Continuous wave (CW) acoustic methods probe standing wave patterns. Current techniques employ cavity resonator cells (sometimes named interferometers), in which the pathlength of interactions of the sonic field with the sample is virtually increased by multiple reflections. Such a 'folding' of the sound path results in a high sensitivity of such devices, so that, at least in a limited frequency range, high resolution measurements on small liquid volumes become possible. This feature permits us to study precious and rare samples, such as special biochemical assays, acoustically.

In the simplest form of a resonator one-dimensional plane waves are set up in a liquid-filled cylindrical cavity between two planar piezoelectric transducers (for thickness vibration) or between a transducer and a passive reflector [7, 81, 130–140]. As the latter often involves unfavourable measurement conditions for the reflected signals, present resonators are constructed with two transducers, one operated as a transmitter and the other one as a receiver. This configuration allows for the direct determination of the complex transfer function $T(\nu)$ of the resonator, e.g. with a network analyser (figure 9) that measures the complex output-to-input voltage ratio $U_{\mathrm{out}}(\nu)/U_{\mathrm{in}}(\nu)$ of the cell. Measurement of both amplitude and phase of $T(\nu)$ is helpful, but not mandatory. Therefore scalar network analysers or level meters, combined with a signal source, can also be used. Profiting from the use of continuous wave signals, modern network analysers provide a very small receiver bandwidth (in the Hz region), yielding a superior signal-to-noise ratio.

Basically the sonic cell is treated as an ideal resonator with pathlength, i.e. transducer distance, x_R and with infinite lateral dimensions and with perfect reflection at the transducer–liquid interfaces; the magnitudes $|r_i|$ and $|r_o|$ of the reflection factors at $x = 0$ and $x = x_R$, respectively, equal 1 (figure 10). The sum

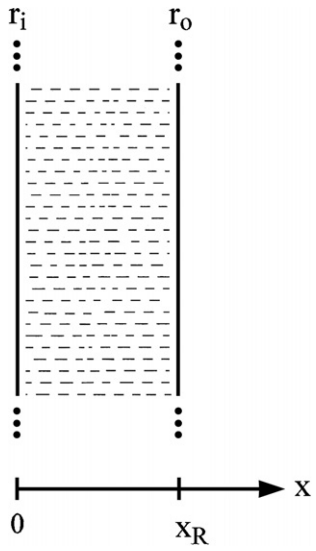

Figure 10. Schematic cross-section of an ultrasonic resonator.

of the primary wave and of all waveforms reflected back and forth at the transducers yields the transfer function as

$$T(\nu) = \frac{U_{\text{out}}(\nu)}{U_{\text{in}}(\nu)} = \frac{U(x_R, \nu)}{U(0, \nu)} = \frac{A}{\sinh(\gamma x_R)}, \tag{21}$$

where A is an amplitude, $\gamma = \alpha_M + \mathrm{i}k_M$ ($\mathrm{i}^2 = -1$) is the complex propagation constant and α_M is the absorption coefficient of the liquid medium. Hence, the amount of the transfer function follows as

$$|T(\nu)| = \frac{|A|}{[\sinh^2(\alpha_M x_R) + \sin^2(k_M x_R)]^{1/2}}. \tag{22}$$

This expression exhibits relative maxima at

$$k_M x_R = n\pi, \qquad n = 1, 2, \ldots. \tag{23}$$

Hence, a series of equidistant resonance frequencies

$$\nu_n = nc_M/(2x_R), \qquad n = 1, 2, \ldots, \tag{24}$$

exists. This relation is frequently used in the determination of sound velocity values from resonator measurements. Below we will discuss the effects from finite lateral dimensions and finite thickness of the transducers ($|r_i|, |r_o| < 1$ and complex r_i, r_o) in real cells.

Due to the nonvanishing absorption coefficient α_M, the transfer function (equation (22)) includes resonance peaks with a finite half-power (−3 dB) bandwidth:

$$\Delta\nu_n = \alpha_M c_M/\pi \tag{25}$$

at the resonance frequencies ν_n. This simple relation, resulting from the development of the resonance curves in a small frequency range around ν_n, indicates the inefficiency of resonator techniques at high liquid absorption, when the standing wave ratio deteriorates. Broad resonance curves enforce a reduced accuracy in the determination of resonance frequencies ν_n and the resulting c_M data. The frequency normalized absorption coefficient $\alpha_M/\nu^2 = 21.28 \times 10^{-15}$ s^2 m^{-1} of water at 25 °C [141] predicts $\Delta\nu_n \simeq 10^3$ Hz at 10 MHz and a 'theoretical' quality factor

$$Q = \nu_n/\Delta\nu_n \approx 10^4. \tag{26}$$

For the critical triethylamine/water system at 17 °C, α_M/ν^2 is about 10^3 larger than the value for water [142], so that a rather broad resonance curve results. The above relations, valid for small α only, estimate $\Delta\nu_n \approx 10^6$ Hz and $Q \approx 10$ for the critical triethylamine/water mixture. Since a low quality factor (<100) obstructs a precise determination of the resonance frequency, absorption restricts the use of resonator cells for sound velocity measurements of liquids at high frequencies. The absorption coefficient of liquids includes a high frequency part $\alpha_{\text{asy}} = B'\nu^2$ that increases proportional to squared frequency [76]. Therefore, the half-power bandwidth of resonances increases towards high frequencies as $\Delta\nu_n = c_M B'\nu^2/\pi$. Because of the (nearly) frequency independent distance $(\Delta\nu_{n+1} - \Delta\nu_n)$ between two resonances in equation (24), neighbouring resonance peaks tend to overlap at high ν. At low frequencies, on the other hand, diffraction, due to the finite diameter of real cells, restricts the usable frequency range of measurements, as will be discussed in section 3.1.

Several methods of sound velocity measurements utilize the interaction of optical waves with continuous ultrasonic waves [143, 144]. In particular, Bragg scattering [145] and Brillouin scattering [146] are challenging for scientific applications, because both methods obtain sound velocity and absorption at hypersonic frequencies ($\nu > 1$ GHz). It is important that spontaneous Brillouin scattering permits us to study liquid samples in complete thermal equilibrium with light scattering by thermal waves. Improved signal-to-noise ratios, however, are reached in Bragg reflection as well as in stimulated [147, 148] and forced [149] Brillouin scattering techniques. In Bragg scattering, a piezoelectric transducer generates an ultrasonic wave (frequency ν) within the liquid; the light from a laser, scattered by the sound wave, is detected and analysed. Stimulated Brillouin scattering induces thermal phonons by a nonlinear effect, based on electrostriction in an intense laser beam. Forced Brillouin scattering utilizes coherent acoustical phonons that are optically generated with the aid of two frequency-tunable continuous wave lasers.

The scheme of a spontaneous Brillouin scattering experiment is sketched in figure 11. According to the Bragg condition, the sonic wavelength λ can be calculated from the angle θ between the incident and reflected light beams and the wavelength λ_L of the laser light as

$$\lambda = \frac{\lambda_L}{2} \arcsin\left(\frac{\theta}{2}\right). \tag{27}$$

Doppler shift leads to a change in light frequency

$$\Delta\nu_L = \pm 2\nu_L \frac{c}{c_L} \sin\left(\frac{\theta}{2}\right) = \nu \tag{28}$$

with $c_L = \lambda_L \nu_L$; ν_L is the light frequency and ν is the frequency of the selected sonic wave. In this way, measurements of $\Delta\nu_L$ and θ allow us to determine c_M, if c_L is known. Because of sonic absorption, the Stokes and anti-Stokes Brillouin lines (figure 11) display a finite half-width:

$$\delta\nu_L = \pi\alpha_M c_M, \tag{29}$$

which can be used to determine the absorption coefficient α_M.

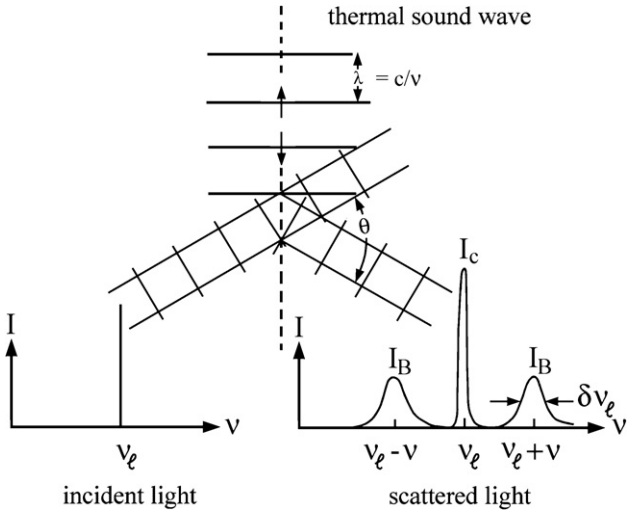

Figure 11. Brillouin scattering by Bragg reflection of laser light from thermal sound waves.

For an estimation of the highest attainable sonic frequency in Brillouin scattering experiments, backscattering conditions, ($\theta = \pi$) as an extreme, are assumed. For visible light (frequency-doubled Nd:YAG laser, $\lambda_L = 532$ nm) in water (refraction index $n_L = 1.33$), a maximum frequency $\nu = 7.4$ GHz results; at that frequency the half-power bandwidth of the Brillouin lines is $\delta\nu_L = 560$ MHz. Separation of these lines from the central Rayleigh line is a challenging task. For a $\Delta\nu_L$ error <1%, an accuracy for the optical frequencies ν_L better than $1{:}10^7$ has to be reached. This is especially important, as according to the Landau–Placzek ratio [144]

$$\frac{I_B}{I_c} = \frac{c_P - c_V}{2c_V}, \tag{30}$$

the intensity I_B of the Brillouin lines is substantially lower than the intensity I_c of the central line. In equation (30), c_P and c_V are the heat capacities at constant pressure and constant volume, respectively. Typically for liquids I_B/I_c is of the order of 10^{-6}. For these reasons, Brillouin scattering is less suitable for routine measurements of liquid sound velocities. In addition, like all optical methods, it is not applicable to opaque samples.

3. Current technical status

3.1. Resonator methods

3.1.1. Cell design criteria. Because of the high sensitivity, even with small sample volumes, from the multiple reflections of sound waves in resonators and because of the advantage of employing continuous wave signals, resonator techniques are preferred for small volume sound velocity measurements at present. For this reason, special attention is given in this review to resonator cell design as well as to resonator data acquisition, evaluation and accuracy.

Real cells differ from ideal resonators in some features. The differences from ideal cell properties have been considered in sonic attenuation spectroscopy for a long time, but only recently in ultrasonic velocity measurements [7]. In order to show accuracy limitations resulting from nonideality, some features are briefly discussed below. Let us first consider the effect from finite acoustical impedance Z_T of piezoelectric transducers, leading to a reflection factor $|r| < 1$ at the liquid–transducer interfaces. For a plane X-cut quartz/water interface the transducer-to-liquid acoustic impedance ratio at room temperature is

$$Z_T/Z_M = (\rho_T c_T)/(\rho_M c_M) \approx 9, \tag{31}$$

leading to an (amplitude) reflection factor magnitude

$$|r| = \frac{Z_T/Z_M - 1}{Z_T/Z_M + 1} \approx 0.8. \tag{32}$$

In equation (31) ρ_T and ρ_M are the densities of transducer and liquid medium, respectively, and c_T is the sound velocity of the transducer material in the direction of wave propagation. Hence, at reflection at the liquid–transducer interface one-fifth of the acoustical wave amplitude propagates into the quartz transducer.

Lithium niobate ($LiNbO_3$—35° rotated Y-cut), on the other hand, is quite attractive for transducers in many ultrasonic applications. Here the impedance ratio with respect to water is $Z_T/Z_M \approx 23$, leading to an increased reflection factor $|r| \approx 0.92$. Another significant difference is the relatively high electromechanical coupling coefficient $K_{LN} = 0.5$ as compared to $K_{XQ} = 0.093$ for X-cut quartz [91]. This coupling coefficient determines the efficiency of energy conversion from electrical to mechanical and vice versa; in consequence devices, including resonators, with lithium niobate transducers exhibit reduced conversion loss or a higher output to input power ratio, often preferred by commercial designers. This feature, originating from a stronger coupling between electrical and mechanical circuits, on the other hand, causes a reduction of Q values near the transducer harmonics; this effect is similar to the Q-reduction of dielectric resonators with close coupling at microwave frequencies.

Assuming nearly ideal reflection at the transducer–air backside interface, it is therefore appropriate to treat the total transfer function

$$T(v) = T_{TT}(v)T_L(v)T_{TR}(v) \tag{33}$$

as a product of the liquid transfer function T_L as well as the transmitter and receiver transducer transfer functions T_{TT} and T_{TR}, respectively. The former can be calculated by analogous application of equation (21); the latter may be considered to differ from one another ($T_{TT} \neq T_{TR}$ [150]). However, it is convenient to use identical transmitter and receiver transducers, getting $T_{TR} = T_{TT}$.

Assuming again infinite lateral dimensions of the cell and neglecting sound absorption within liquid and transducers, the series of resonance frequencies follows as [98]

$$\nu_n = \nu_{n\ \mathrm{ideal}} + \frac{c_M}{\pi x_R} \arctan\left[\frac{Z_M}{Z_T}\cot(\pi\nu_n/\nu_T)\right], \quad n = 1, 2, \ldots, \tag{34}$$

where $\nu_{n\ \mathrm{ideal}}$ is the nth resonance frequency according to equation (24), the second term on the right-hand side is a correction term for the acoustic field within the transducers, i.e. their complex reflection factor, $\nu_T = c_T/(2d_T)$ is the

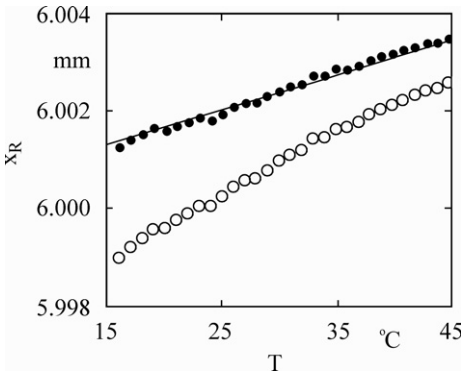

Figure 12. Length x_R of a resonator cavity versus temperature T (frequency 2.3 MHz; reference water [7]). ○○○: data neglecting finite transducer thickness (equation (24)). ●●●: data from principal resonance frequencies and rigorous evaluation (equation (34)). ———: calculated thermal expansion (equation (35)) with $x_{R0} = x_R(300\ \mathrm{K})$ and $\Delta T = T - 300\ \mathrm{K}$.

transducer fundamental frequency for thickness vibrations (d_T: transducer thickness).

Equation (34) can be used to determine the acoustic length x_R from resonance frequency measurements with a reference liquid of well-known sound velocity c and acoustical impedance (ρc). Figure 12 shows the temperature dependence of a resonator cell length, determined with water as a reference liquid. Data obtained from equation (34) agree well with the temperature variation of x_R, calculated from the thermal expansion coefficient of the spacer, which defines the distance between the transmitter and receiver transducer in the cell $x_R = x_{R0}\ (1 + \alpha_{\mathrm{th}}\Delta T)$ with ΔT temperature shift and $\alpha_{\mathrm{th}} = 1.65 \times 10^{-5}\ \mathrm{K}^{-1}$ thermal expansion coefficient for stainless steel. The length values obtained from the ideal-resonator formula (equation (24)) are smaller. The relative difference at room temperature is $(x_R - x_{\mathrm{ideal}})/x_R = 3.3 \times 10^{-4}$, significantly larger than the error limit claimed in present sound velocity measurements. However, if the simple relation (24) is used instead of equation (34) in both the determination of the cell length and the evaluation of the sample measurements, the effects from the incomplete description of the sound field will largely cancel, if sound velocity and density (thus acoustical impedance) of the reference agree with the corresponding sample data.

The frequency-dependent (complex) reflection factor at the liquid–transducer interfaces leads to a non-equidistant distribution of resonance frequencies (equation (34)). The difference between subsequent resonance frequencies, often used for resonator data evaluation, is given by [81, 98, 136, 139]

$$\nu_{n+1} - \nu_n = \frac{\nu_{n\,\mathrm{ideal}}}{\pi} \arccos\left[\frac{\left(g_{n+1}^2 - 1\right)\left(1 - g_n^2\right) - 4 g_{n+1} g_n}{\left(g_{n+1}^2 + 1\right)\left(g_n^2 + 1\right)}\right], \quad n = 1, 2, \ldots, \tag{35}$$

where

$$g_j = \frac{Z_l}{Z_T} \arctan(\pi \nu_j / \nu_T), \qquad j = 1, 2, \ldots. \tag{36}$$

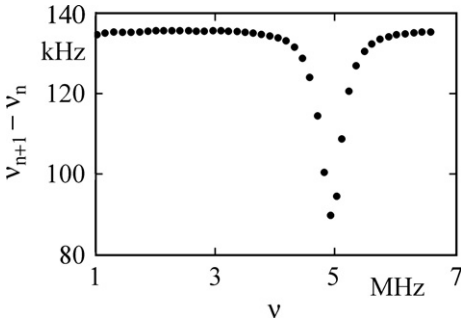

Figure 13. Resonance frequency difference $(\nu_{n+1} - \nu_n)$ versus ν_n for cavity resonator with water at 25 °C (X-cut quartz transducers, ∅ = 20 mm, thickness $x_T = 0.57$ mm, $\nu_T = 5$ MHz).

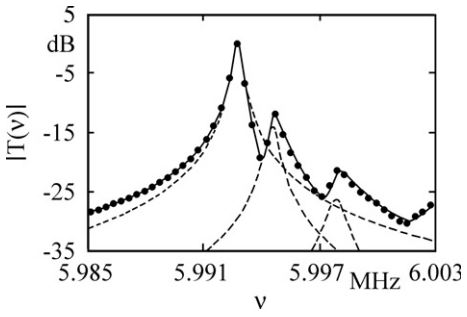

Figure 14. Transfer function magnitude for a water (25 °C) filled resonator cell (X-cut quartz transducers, ∅ = 20 mm, $\nu_T = 4$ MHz; - - - -: transfer functions of three Lorentz terms, equation (39); ——: sum of these three terms).

Figure 13 indicates a particularly strong dependence of the resonance frequency difference at ν_T. The same effect follows for the harmonics $(m + 1)\nu_T$, $m = 1, 2, \ldots$. Around these frequencies sound velocity measurements should be avoided, especially when equation (24) is used to calculate c_M values from $(\nu_{n+1} - \nu_n)$ data.

Real cells also differ from ideal cavity resonators in their finite lateral extension. This leads to a mode spectrum exhibiting higher order modes, in addition to the principal resonances, and also to noticeable diffraction effects at lower frequencies. As illustrated by the resonator transfer function in figure 14, the acoustical field of circular cylindrical resonators with plane faces involves radial modes ('satellites') with resonance frequencies $\nu_{n\,k}$ larger than those of the principal mode (ν_n). The frequency distance of the modes is given by the relation [151]

$$\nu_{nk} - \nu_n = \frac{1}{8\nu_n}\left(\frac{c}{R}\right)^2 \left(k + \frac{1}{2}\right)(k - 1), \quad n, k = 1, 2, \ldots \tag{37}$$

(R: cell radius). At sufficiently small absorption ($\alpha_M\ x_R < 0.1$), the transfer function near a principal resonance can be developed as a sum of Lorentz terms:

$$|T(\nu)| = \sum_{k=0}^{K} \frac{A_k}{1 + \mathrm{i}\frac{2}{\Delta\nu_{hk}}(\nu - \nu_k)}. \tag{38}$$

Here $k = 0$ denotes the principal resonance and $k = 1, 2, \ldots$, the higher order satellite modes. Parameters A_k, ν_k and

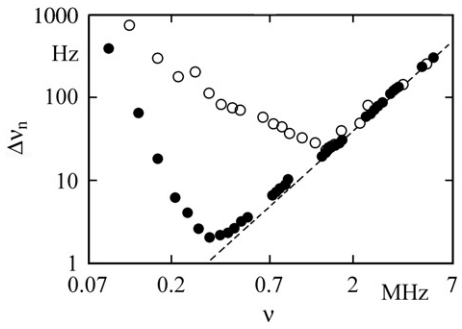

Figure 15. Half-power bandwidth spectrum $\Delta\nu_n$ of biplanar (○, ∅ = 70 mm, $x_R = 14$ mm) and plano-concave (●, ∅ = 80 mm, $x_R = 19$ mm) resonator, filled with water at 25 °C versus ν [157]. - - - -: attenuation term $c\alpha/\pi$ for water, i.e. $\Delta\nu_n$ of an ideal (diffractionless) resonator (equation (40)).

ν_{hk} are the amplitude, resonance frequency and half-power bandwidth, respectively, of the kth resonance peak. Careful consideration of the radial modes is mandatory for accurate sound velocity measurement, since the absorption coefficient of the reference liquid is usually different from that of the sample and, therefore, influences of higher order modes on the principal resonance are unequal. Typically, the deviation $\Delta c/c$ for satellite mode influences is in the order of 10^{-6} to 10^{-5}. In practice it is the strong overlap of higher order modes with the principal resonances that limits the resonator method at high absorption coefficients.

At lower frequencies, diffraction effects originate from the finite diameters of cell and sound beam. Labhardt and Schwarz [81] have published a relation for the half-power bandwidth of the principal resonances of real resonators:

$$\Delta\nu_n = \alpha_M c_M/\pi + Y_2\nu^{-2} + \mu c_M/\pi \qquad (39)$$

in which, in correspondence with the expression for the ideal cell, equation (25), the first term on the right-hand side represents the liquid absorption. The second term accounts for the energy loss from diffraction, with the parameter

$$Y_2 = \frac{0.147}{\pi}\frac{Z_W}{Z_M}\left(\frac{c_M}{R_{\text{eff}}}\right)^3, \qquad (40)$$

depending on the sidewall/liquid impedance ratio Z_W/Z_M, the effective sonic beam radius R_{eff} and the sound velocity of the liquid medium c_M. Since Y_2 is proportional to c_M^3, the sound velocity of the reference liquid should be well matched to that of the sample, if measurements are made at frequencies at which diffraction effects contribute noticeably to ν_n. The third term on the right-hand side of equation (39) includes the radiation loss from the back face of the piezoelectric transducers into air; it can be reduced by evacuating the back space of the transducer. Radiation loss, however, is influential only near ν_T and its odd overtones $(2m+1)\nu_T$; these frequencies are normally avoided in resonator measurements.

The ν^2 dependence in the half-power bandwidth $\Delta\nu_n$ (equation (39), figure 15) restricts biplanar resonator measurements at low frequencies. In order to shift the range of unfavourably large $\Delta\nu_n$ values to lower frequencies, the focussing effect of concavely shaped end faces is utilized

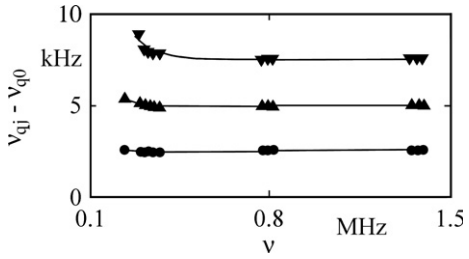

Figure 16. Differences between resonance frequencies of higher order modes $\{\nu_{qj}\}$ and of the corresponding principal mode $\{\nu_{q0}\}$ for a biconcave resonator filled with water at 25 °C [158]. Cell ∅ = 95 mm, $\nu_T = 2$ MHz, transducer curvature radius $R_c = 2$ m.

in sound velocity measurements [152–160]. Biconcave [152, 153, 158–160] and plano-concave [154–157] cells are employed. Most of the latter use a plane piezoelectric transducer and a concavely shaped (passive) reflector [154–156]. A device with a concavely ground, finely polished X-cut quartz transducer disc has also successfully been used [157]. In order to reach lowest minimum frequencies with adequate Q in resonator measurements, a comparatively large cell radius R is required. With a larger sample volume (about 100 ml), the minimum in the half-power bandwidth curve has in fact been shifted to lower frequencies (figure 15); measurements down to 80 kHz become possible with plano-concave or biconcave cells. Small biconcave cells, requiring millilitre sample volumes only, cannot reach such low frequencies but offer other favourable properties [160], such as equidistant resonance frequency differences (figure 16), enabling biconcave cell measurements at higher frequencies than with corresponding biplanar resonators [160], for which higher order mode peaks and principal resonance peak converge with increasing ν. An inestimable feature of plano-concave and biconcave resonator cells is their impassiveness with respect to small mechanical disturbances. The focussing effect of the faces reduces the risk of a disturbance in transducer parallelism when the sample is exchanged for the reference liquid. Temperature-dependent measurements, sometimes accompanied by mechanical cell strain, are also facilitated in focussing resonators.

3.1.2. Multi-layer cells. Cavity resonators require cell wall materials resistant to the sample liquid. The facing piezoelectric transducers are usually covered by gold on chrome layers, establishing the electrical electrode and ground. The cell jacket is favourably made from glass or plexiglass, but stainless steel or titanium spacers are also used. In many applications, liquids can interact chemically with the cavity walls; in particular, corrosion of chrome is observed when the gold layer is not absolutely tight. In scientific applications selected materials, matched to the particular liquid samples, are employed. In many technical and industrial applications, cavity walls are entirely non-metallic and non-piezoelectric. In such devices commercially available precision-type glass cuvettes for optical use are employed, forming the cavity and enclosing the liquid specimen. A construction is shown in figure 17. Here, the piezoelectric transducers must be

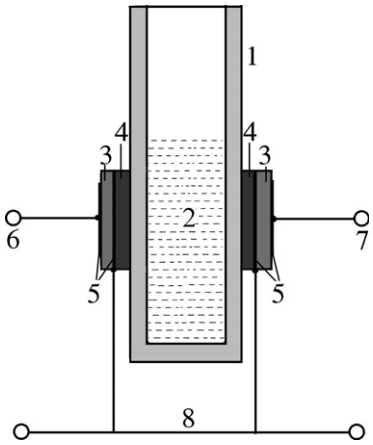

Figure 17. Schematic sketch of a cuvette cell [5, 161]. 1: resonator chamber body; 2: sample liquid; 3: piezoelectric transducer; 4: intermediate layer (coating) for acoustic contact and, possibly, acoustic impedance match; 5: metallic layers for electrical contact; 6 and 7: connections to signal generator and receiver, respectively; 8: electrical ground.

acoustically coupled to the outside of the cuvette. They may be removable in order to facilitate an exchange of the cuvette for cleaning and refilling procedures. Acoustical contact can be improved by an additional coating, i.e. an intermediate layer for impedance matching.

A drawback of such multi-layer cells is the additional reflections between different interfaces. Thereby, the resonance spectrum and its theoretical analysis are considerably complicated. In practice, frequency-dependent correction coefficients $\beta^*(\nu)$ and $\gamma^*(\nu)$ are introduced [5, 162, 163] in order to expand the applicability of the ideal-resonator equation (24)

$$c_M = 2x_R(\nu_{n+1} - \nu_n)(1 + \beta^*). \tag{41}$$

Often sound velocity measurements only aim at the velocity increment δc_M with respect to a reference value; in this case, a good approximation is reached with the corresponding frequency increment $\delta\nu_n$ for a particular resonance and a correction factor

$$\delta c_M/c_M = (1 + \gamma^*)\delta\nu_n/\nu_n. \tag{42}$$

These empirical correction coefficients have to be found by calibration measurements with liquid standards of precisely known velocity. In correspondence with equations (34) and (36) for traditional, much simpler three-layer cavities, both the sound velocity and the acoustical impedance of sample and the reference liquid should be very close in order to simulate the resonance frequencies accordingly. This condition is difficult to realize. Favourable conditions, however, exist quite often for dilute solutions with the solvent as a reference, offering close velocity and density parameters.

3.1.3. Data recording and evaluation. Today it is common practice to use network analysers or impedance analysers for multi-frequency measurements, needed to obtain the total transfer function T (equation (33)). Knowledge of $T(\nu)$ around a resonance frequency ν_n permits us to eliminate the disturbance from higher order modes for accurate determination of ν_n. Usually, $T(\nu)$ is analysed in terms of a sum of Lorentz functions (equation (38)).

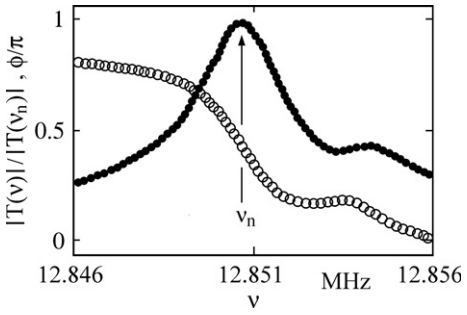

Figure 18. • Magnitude $|T(\nu)|$ and ○ phase Φ (ν) of the transfer function $T(\nu)$ of a cylindrical cavity resonator with plane faces, filled with water at 20 °C [136]. Shown are principal resonance ($\nu_n = 12.850\,76$ MHz) and first radial mode.

Measurement and analysis of $T(\nu)$ offers the possibility of detecting asymmetries in resonance curves from electromagnetic crosstalk [136] and irregularities in the partial transfer functions T_{TT} and T_{TR} of the transducers. In principle, T_{TT} and T_{TR} can be determined by reference measurements with liquids of well-known parameters. For identical planar plate transducers with fundamental frequency ν_T [136, 138]

$$T_{TR}(\nu) = T_{TT}(\nu) \equiv T_T(\nu) \tag{43}$$

and

$$T_T(\nu) = A\exp(-B\nu)[1 - \mathrm{i}D\cot(\pi\nu/(2\nu_T))]^{-1}. \tag{44}$$

At $\nu \neq n\,\nu_T$, $n = 1, 2, \ldots$, this relation can be approximated by

$$T_T(\nu) = A\mathrm{e}^{-B\nu}. \tag{45}$$

Vector network analysers and impedance analysers provide both amplitude $|T|$ and phase Φ of the total transfer function $T(\nu)$, as shown in figure 18. In this way an advanced resonance frequency determination becomes possible.

Because of microprocessor-controlled measuring routines today multipoint measurements offer high accuracy with quick and easy performance. Commercial, multi-purpose network analysers, however, are rather complex and too costly for routine-type measurements of transfer functions; they can be substituted by other low cost devices [5, 7]. A block diagram of a system determining resonator input and output voltages and its phase difference is shown in figure 19. The device offers two channels for a sample and a reference cell. In technical applications, velocity measurements are often performed simultaneously in several cells; in this way, identical temperatures in the samples can be reached. Such systems allow an extension of additional sound channels.

The electronic circuit is based on the direct digital frequency synthesis (DDS) technique. One synthesizer (2a in figure 19) provides the sinusoidal measuring signal (frequency ν) and the other one (2b) provides the local oscillator signal (frequency ν + 10 kHz) for superheterodyne mixing and amplification. The measuring signal is fed to

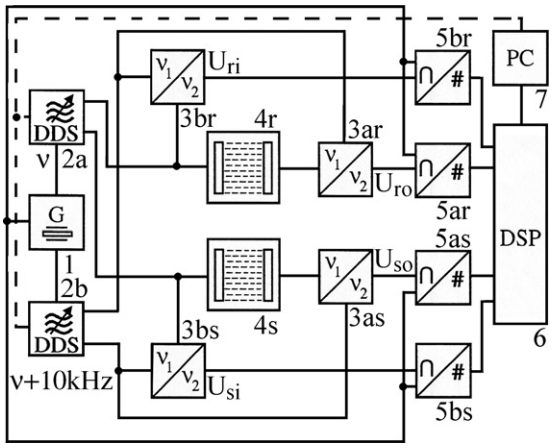

Figure 19. Simplified block diagram for a dual channel electronic system to determine complex transfer functions of twin resonator cells [7]; broad-band attenuators and amplifiers are omitted; s and r refer to the sample and reference channel, respectively. 1: quartz controlled 50 MHz clock; 2a, 2b: direct digital synthesizer ($\nu_{max} =$ 25.00 MHz); 3a, 3b: RF mixer; 4: twin resonator cell; 5a, 5b: A/D converter; 6: digital signal processor board, implemented in 7: computer.

the input transmitters of both cells; the output signals are processed in two mixers 3as and 3ar, respectively, together with the local oscillator signal. The resulting IF signals (IF: intermediate frequency 10 kHz) are proportional to the magnitudes of the cell output voltages U_{so} and U_{ro}. After analog/digital conversion, the IF signals are processed in a digital signal processor board (DSP). This DSP board also receives the reference signals, which are proportional to $|U_{si}|$ and $|U_{ri}|$, respectively, of the cell input voltages. These voltages are derived from part of the measuring signal that is directly mixed (3bs, 3br) with the local oscillator signal.

The real and imaginary parts of $U_o\ (\nu)/U_i\ (\nu)$ for both the measuring and the reference channels are obtained by sampling U_o in phase with U_i and also at a $\pi/2$ phase shift which is equivalent to a delay $\Delta T_{IF} = 25\ \mu$s in the 10 kHz IF signal. In order to reach a frequency stability better than 0.1 Hz and a phase jitter below 0.01°, the DSG generators (2a, 2b) and the analog/digital converters (5a, 5b) are controlled by a quartz-stabilized 50 MHz clock (1).

It has already been mentioned that temperature control is of primary importance for high precision sound velocity measurements. Laboratory equipment manufacturers provide microprocessor-controlled liquid circulators with a temperature stability near 0.01 K; fluctuations of 0.01 K cause relative velocity variations in water of about 2×10^{-5} (figure 7). Such variations are indeed tolerable in many cases; for example they are sufficiently small for an investigation of bilayer membrane systems, as shown with sound velocity profiles in figure 2. Accuracy is enhanced by using twin cells [57] for a sample and a reference liquid; with both cavities inserted in the same metallic block, the temperature difference becomes smaller than the fluctuations in the thermostat fluid. Differences close to 10^{-4} K between the two cavities have been reported for a temperature stability near 0.01 K in the block.

An improved temperature regulation with respect to adjustment and stability is reached with Peltier elements. In order to get full advantage of this technique the Peltier elements should have channels for circulation of a pre-thermostated fluid, and the control electronics should also be kept at rather constant temperature [7]. It is advisable to place the cell and the controls in a thermostatic box.

In order to keep temperature fluctuations small during a measurement period, a short measuring time is helpful. Therefore an efficient algorithm has been developed [7], delivering the complex transfer functions of both cells for 200 frequency points within 6 s.

Frequently, only the velocity difference $(c_s - c_r)$ between the sample and reference liquid is of interest. Examples are studies on dilute solutions of certain biomolecules (figure 2). High resolution data are obtained differentially in a twin-cell resonator. For absolute c-values, however, the reference path is just used to correct temperature values, using the known gradient $\mathrm{d}c/\mathrm{d}T$ of the reference liquid. Resonator length x_R calibration is performed with the resonance frequencies of a reference liquid with standardized velocity, such as water. Likewise, the correction factors β^* (or γ^*) for a simplified evaluation of multilayer-cell data are determined in this way. The experimental transfer function $T(\nu)$ data are stored in the process control computer (7 in figure 19) and deconvolved to include the effects from the transducer transfer functions (equations (33), (44), (45)) and from higher order modes (equation (38)). This analytical procedure, using nonlinear regression, yields the principal resonance curve in terms of a Lorentz function and the correct resonance frequency.

3.1.4. Resolution and accuracy. Using modern network analysers with an adequate frequency resolution combined with measuring and data fitting procedures, as described before, allows a determination of resonance frequencies ν_n with errors below 0.1 Hz. In this way, inaccuracies of ν_n values in the MHz frequency range result in relative velocity errors $\Delta c/c \leqslant 2 \times 10^{-7}$.

It has been already underlined that temperature fluctuations are a critical element in high-precision c measurements. An accuracy of $\Delta c/c = 2 \times 10^{-7}$ can be reached only with a temperature stability better than 10^{-4} K (figure 7). Such small temperature fluctuations can be realized but need a long stabilization time, intolerable for some applications. Twin cells with a stainless steel spacer ring have been reported to require about 20 min to reach fluctuations $\Delta T < 3$ mK [7]. Small sample volumes <1 ml and stirring of the liquid reduce temperature gradients and equilibrium time, leading to improved temperature stability after an acceptable waiting time.

Another critical element in such measurements are the liquid wetting properties and the formation and persistence of small gas bubbles, even in carefully degassed liquids. Figure 20 shows the relative velocity differences $(c_1 - c_2)/c$ for two runs of a phospholipid vesicle suspension (similar to that in figure 2), the cavity filled twice with the same sample; the differences amount to about $10^{-4}\ c$ and are particularly large near the transition temperature T_m, where the surface active

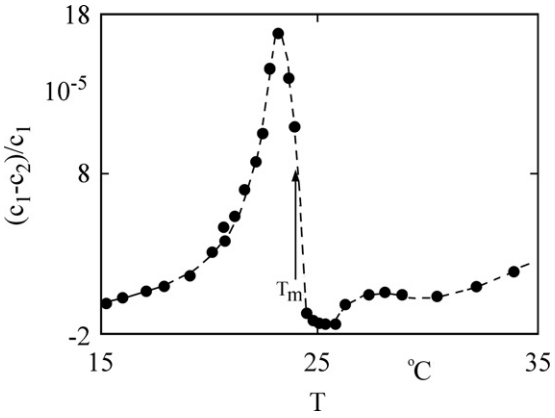

Figure 20. Relative difference of sound velocity data as a function of temperature T from two runs for resonator measurement. The cell has been cleaned in between and refilled with the same sample (aqueous vesicle solution of 1,2-dimyristoyl-L-3-phosphatidylcholine). T_m: phase transition temperature of phospholipid. - - -: interpolating line to guide the eye.

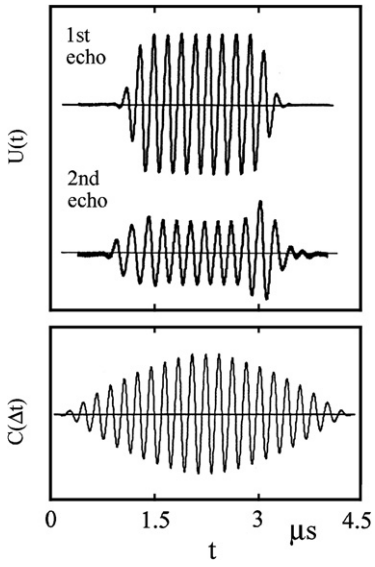

Figure 21. Waveforms $U(t)$ in pulse correlation measurements and cross-correlation function $C(\Delta t)$ of the first and second echoes [111].

colloidal solution undergoes structural changes. Therefore, repeated scans are recommended for extra accurate absolute c data. We want to mention that aqueous carbohydrate solutions also exhibit complex wetting behaviour. Reliable ultrasonic parameters, velocity and attenuation as well, often require multiple, i.e. repeated, filling procedures.

In summary, it can be said that sound velocity measurements with resonators are most sensitive with small sample volumes. The obtainable experimental accuracy depends crucially on the temperature stability provided by the control system. In addition individual sample properties, e.g. surface tension and wetting behaviour, are quite influential.

3.2. Propagating wave methods

3.2.1. Transit time measurements. Many applications employ techniques based on the time delay (equation (15)) between two pulse-modulated waveforms that have been transmitted through a specimen cell or are reflected from the back side of a cell. Often such techniques are named 'pulse time of flight'. The sing-around methods, mentioned in section 2.2, determine Δt_{tot} in a special way; also common are direct transit time measurements with a timer start/stop configuration [54] and pulse-echo-overlap methods [109]. Most methods use sharp pulses and determine the group velocity c_g.

For pulse-transition and pulse-echo measurements as well the sensitivity can be enhanced using multiple reflections with the relation

$$\Delta t_{\mathrm{tot}} = 2n\Delta x/c_g + t_c, \qquad n = 1, 2, \ldots, \tag{46}$$

with n denoting the number of echoes, Δx the acoustic cell length and t_c again the electronic time delay. In contrast to resonator techniques, however, no large n values ($n > 10$) are possible for pulse measurements, because—especially at significant attenuation and dispersion in the sample—reflected pulses become more and more distorted when n increases. Due to this restriction for n pulse measurements with a resolution $\Delta c_g/c_g \approx 10^{-6}$ (as obtained with resonator measurements for phase velocities) longer pathlengths and higher sample volumes are required; cell lengths of 40 mm [6] or even 60 mm [111] have been reported. This necessity for larger volumes makes resonators attractive for acoustic investigations of expensive or scarce sample solutions.

The main error source in transit time measurements is the varying trigger point delay, due to pulse deformation from bandwidth limitations of the electronic circuit and the piezoelectric transducers and, in addition, from frequency-dependent liquid absorption and dispersion. The variance with respect to the exact trigger point can be reduced by an automatic pulse correlation measurement system [111]. It derives the sound velocity from the time interval Δt between the first and the second echoes of reflected pulses by means of the correlation function

$$C(\Delta t) = \int U(t + \Delta t)U(t)\,\mathrm{d}t, \tag{47}$$

where U is the receiver signal voltage. Figure 21 shows the waveforms of the echoes and also their cross-correlation function C with a positive maximum at each

$$\Delta t^n_{\mathrm{max}} = \Delta t + n/\nu, \qquad n = 0, \pm 1, \pm 2, \ldots, \tag{48}$$

(ν: sinusoidal signal frequency). Since an error in n by 1 or -1 leads to a significant difference in c, it is simple to eliminate any ambiguities of the time shift $\Delta t^n_{\mathrm{max}}$. The resolution of the pulse correlation method, which is much faster than the conventional sing-around method and therefore offers a better temperature stability, reaches $\Delta c/c \approx 10^{-6}$ [111]. A theoretical analysis for applications on absorbing and dispersive media has also been published [164].

The aforementioned techniques, using broadband pulsed ultrasonic signals and fast Fourier transform (section 2.2), have been developed further to yield the phase velocity of the sample as well as the absorption coefficient and the specific acoustic impedance in a frequency range of 0.3 to 6 MHz [165] and also

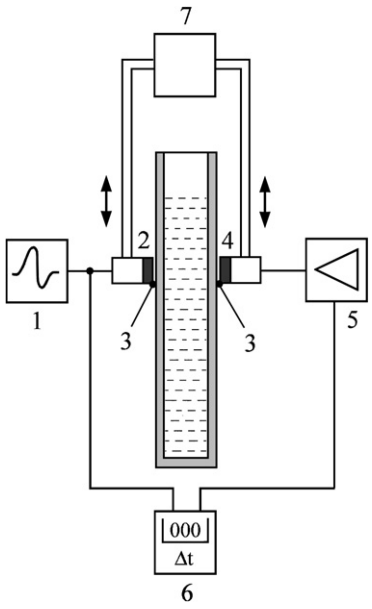

Figure 22. Schematic diagram of an ultrasound scanner [166]. 1: signal generator, 2: transmitter transducer, 3: silicone oil film, 4: receiver transducer, 5: receiver, 6: timer counter, 7: vertical stepper motor.

between 1 and 14 MHz [42]. Frequency scanning ultrasonic pulse-echo reflectometers have been designed with [42] and without [165] an additional reference cell for a comparison (differential) mode of operation. A relative error $\Delta c/c \approx 1$–3×10^{-4} [42] has been estimated for an existing set-up. A limitation of this method is the variation of the actual frequency range, depending on the sample properties and the available time domain echo signals.

An ultrasonic velocity and absorption scanner has been designed to indicate a destabilization of colloidal systems, much earlier than possible by visual observation [166, 167]. The instrument is based on time-of-flight measurements, using a time counter to determine the delay time for pulses transmitted through the cell. The main attraction of the scanner is the pair of ultrasonic transducers, which may be stepped down by a pair of optically parallel glass windows between which the liquid sample is held (figure 22). Silicone oil is used to provide the acoustic coupling between the transducers and the glass discs, respectively. For reproducible acoustic coupling the thickness of the oil film has to be controlled closely, using a metering pump and a well-defined pressure on the transducers against the glass walls [166]. The ultrasound scanner has to be operated in a frequency range between 0.6 and 10 MHz, using two pairs of transducers with fundamental frequencies 2 and 5 MHz. Temperature stability within ± 0.1 K was reached by placing the device in an air-cooled cabinet. So far the accuracy of sound velocity is about 1 m s^{-1}, corresponding to a relative error $\Delta c_g/c_g = \pm 7 \times 10^{-4}$; the sensitivity is one order of magnitude higher [166].

3.2.2. Brillouin scattering. For translucent samples Brillouin scattering techniques likewise allow measurements of the sound velocity in liquids, as well as in gases and solids, in a broad frequency range (section 2.3). In order to reach the high spectral resolution necessary for an analysis of the scattered light spectrum (figure 11), narrow-band lasers and high-contrast spectrum analysers are applied. Multi-pass Fabry–Perot interferometers are most commonly used for the spectral decomposition of the scattered light [168–170], yielding experimental errors $\Delta c/c \approx \pm 0.01$ in sound velocity measurements.

Most limitations of spontaneous and stimulated Brillouin spectrometry are nevertheless imposed by the interferometers. Alternative methods with an increased signal-to-noise ratio are therefore applied. With stimulated Brillouin gain spectrometry [171, 172] and forced Brillouin spectrometry [149], two laser beams with different frequencies are crossed in the sample. When, in the stimulated gain experiment, the frequency difference between intense pump beam and weak probe beam equals the Brillouin frequency, energy is transferred from the high frequency to the low frequency beam through Brillouin-induced four-wave mixing. Frequency tuning of one beam with respect to the other one permits us to generate a Brillouin gain spectrum with a frequency resolution depending only on the laser linewidths. Spectral resolution better than 7 MHz has been reported [149]. Forced Brillouin spectrometry utilizes coherent phonons, which—due to the thermal expansion of the light-absorbing liquid—are resonantly generated by the frequency tunable lasers [149]. Forced Brillouin spectra equal spontaneous Brillouin lines, but they offer a significantly improved signal-to-noise ratio. The favourable signal-to-noise ratio and the frequency resolution have been further increased by a phase-coherent light scattering method, allowing us to record complex Brillouin spectra. The resolution of this method has been claimed to be about 100 times better than that of a Fabry–Perot interferometer [173], offering superior accuracy in sound velocity measurements up to 10 GHz.

Superheterodyne light beating spectrometers have been proposed [99, 174] in close correspondence to superheterodyne techniques used at radio and microwave frequencies. The method involves mixing of light from two specially designed and thermally coupled lasers with a frequency overlap. Single axial mode continuous wave output Nd:YAG lasers with monolithic ring resonators generate signals with a jitter below 150 kHz s^{-1}; they provide an electronic tuning range of 10 GHz, so that the beat signal can be processed with an electronic spectrum analyser. In this way, sound velocity measurements are possible in a wide frequency range from 10 MHz to 10 GHz with a frequency resolution of 300 kHz, which is set by the short-time coherence between the two lasers [174].

Brillouin scattering measurements may be complemented by wavelength determinations of ultrasonic and hypersonic signals within the sample, utilizing the ripple structure in the transfer function of variable pathlength cells (figure 23).

3.2.3. Measurements at high hydrostatic pressure. Knowledge of liquid sound velocities as a function of temperature and pressure is of great importance for fundamental theories of liquids and also for the validation of thermodynamic models. In addition such velocity

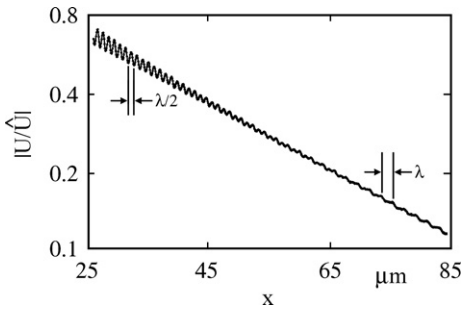

Figure 23. Semi-logarithmic plot of the receiver voltage ratio $U(x)/\hat{U}$ versus sample thickness x [175]; $\hat{U}$: reference voltage, independent of x. Pulsed wave transmission measurements at 790 MHz, performed with a broadband hypersonic cell [176]. ——: graph of the theoretical transfer function. The signal shows a characteristic ripple with periodicity $\lambda/2$ at small x and λ at larger x. The former is due to multiple reflections in the cell; the latter follows from the superposition of the acoustical signal and electrical crosstalk.

data are useful in many fields of technology, e.g. the extraction of oil/gas mixtures from natural oil resources at elevated temperatures and pressures, and also in deep ocean sonography. Sound velocity measurements based on a pulse-echo technique are available for pressures up to 100 MPa and temperatures up to 420 K [9, 11, 177, 178]. Time-of-flight measurements are performed using sharp pulses that are radiated in opposite directions from both faces of a piezoelectric transducer disk; the transducer is located between two reflectors with distances x_1 and x_2, respectively; the echoes from both reflectors are then received by the piezotransducer. The pulse lengths are chosen to ensure a clear separation of the reflected pulse forms at given c_g, x_1 and x_2. From the delay time difference Δt between the first echoes from both reflectors, the group velocity is calculated as

$$c_g = 2|x_1 - x_2|/\Delta t. \tag{49}$$

Here, experimental errors below $\Delta c_g/c_g = 10^{-4}$ have been reached [11].

Alternatively, angle-dispersive Brillouin spectrometry has been applied for high-pressure sound velocity studies [179]; in this investigation relative velocity errors have been near 0.1, but are distinctly smaller than the velocity changes from pressure variation.

3.2.4. Signal processing. Most propagating wave methods for high resolution sound velocity measurements employ conventional signal processing techniques. As mentioned before, correlation functions are used (equation (47)) for the precise determination of the time interval between the first and the second echoes of sharp pulses in terms of the sound velocity dispersion and the frequency-dependent sonic attenuation coefficient [42, 58, 119]. Gating, up-sampling, Hilbert transforming and enveloping [119] are used for an enhancement of the centre of waveforms, increasing the precision in the sound velocity determination from multi-frequency pulse devices. Short-time Fourier transform has been applied recently in a time–frequency analysis of pulsed-signal amplitude data [180]. Again, the aim was information about the ultrasonic dispersion and attenuation properties of samples.

In related measurement modalities wavelet transforms, which may be considered an upgrade of the short-time Fourier transform, have been developed as a valuable tool for noise and speckle reduction, boundary enhancement and image compression. Applications are to be found in all ultrasonic imaging techniques [181–185], such as medical sonography [186–190], scanning acoustic microscopy [191], pattern detection [192, 193], and in non-destructive testing and sample classification [194–197]. Wiener filtering and autoregressive spectral extrapolation [198] as well as maximum non-Gaussianity parameter estimation [199] of echo signals have been applied for an enhancement of the signal-to-noise ratio and a proper consideration of pulse shape distortions. Hence, these transformation and filtering procedures enable a more accurate determination of the pulse time of flight. In the present applications, an increased spatial resolution and thus a higher accuracy in the position estimation of discontinuities in the acoustical impedance follow thereby. Noise reduction and improved pulse shapes could, on the other hand, help to further increase the accuracy of sound velocity measurements.

Wavelet transforms have been applied to ultrasonic pulse-echo measurements for the characterization of the freezing behaviour of orange juice [200]. The wavelet analysis provided the velocity dispersion in the reasonable frequency range from 500 kHz to 4 MHz.

Sound velocity measurements may be also used to predict process states. For such predictions, artificial neural networks are suitable tools to implement scenarios for the anticipated process development. Artificial neural networks have already been processed for the compensation of the secondary effect, especially of the temperature influence during beer fermentation [201]. Likely predicting abilities of sound velocity data are already applied in industry to optimize production logistics.

4. Measurement applications

The potential of sound velocity measurements for non-invasive, non-destructive sample characterizations has stimulated broad fields of applications, which globally may be subdivided into three categories.

(i) High resolution sound velocity measurements provide information about sample property variations as a function of time or other parameters, such as temperature, hydrostatic pressure, pH or enzyme concentration. The ability to analyse opaque samples and the small volume required have established c measurements in numerous areas of fluid analysis and process control. Favourable attributes of sound velocity measurements for monitoring sample variations may be illustrated by the simple determination of the critical micelle concentration (cmc) of a cationic surfactant/water system. Figure 24 shows the sound velocity c, density ρ and electrical conductivity σ of the n-decyltrimethylammonium bromide/water system as a function of surfactant concentration C. Among the

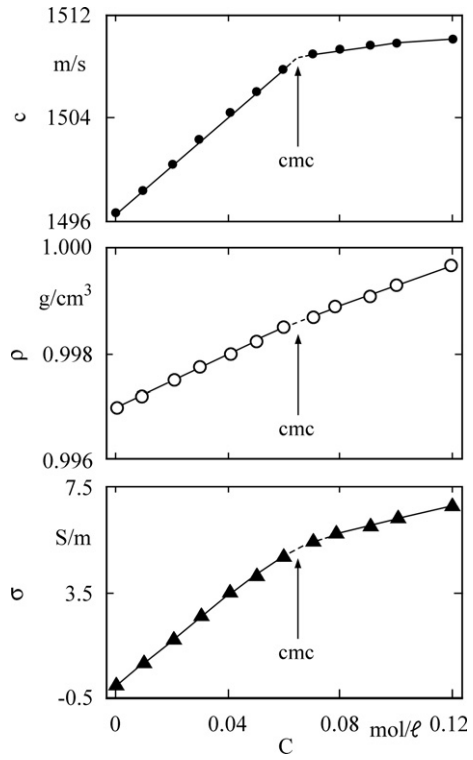

Figure 24. Sound velocity c, density ρ and electrical conductivity σ of n-decyltrimethylammonium bromide/water solutions at 25 °C displayed as a function of surfactant concentration C [202].

three parameters, c exhibits the sharpest bend at the cmc and thus permits the most accurate determination of it. The clear indication of sample property variations by c is utilized in process monitoring and in control systems. A prominent example is the treatment of milk, during which c measurements help to analyse the homogenization procedure, to reach a favourable droplet size and to monitor the status of rennet coagulation as a step in cheese manufacturing [58, 59, 68, 69, 203]. Related examples are the control of gelation profiles during yoghurt fermentation [66, 204] and monitoring the sedimentation for the control of flocculation processes. Studies on compressibility changes of proteins by means of velocity and density measurements have found increasing attention [205, 206].

(ii) The high sensitivity with respect to structural changes in liquids (figure 24), the small sample volume (<1 ml) and the chance to evaluate nontransparent samples make sound velocity an excellent parameter for studies on phase diagrams of complex liquids, e.g. colloidal solutions and emulsions. An illustrative example is the binodale in critically demixing systems; these exhibit a bifurcated c_M versus T relation beyond the phase transition temperature, due to the formation of two phases [207]. Often c_M is not just the direct indicator for a phase transition, but also allows for an analysis in terms of rather sophisticated physical properties, yielding mechanical and thermodynamical parameters [85, 208], droplet diameters [4] and information on solvation effects [41, 209].

(iii) Many applications, especially in basic research, aim at the indication of changes not only in the sample state but also in molecular relaxation processes. Such studies need frequency-dependent sound velocity data, as shown e.g. in figures 1 and 3. In addition to classical relaxation phenomena, addressing fast chemical reactions in solutions [70–80], the critical dynamics of binary and ternary mixtures near the demixing point—highlighting conceptions of universality, scaling and power laws [142, 207, 210–213]—is being investigated by sonic spectrometry. Also of great interest are the frequency-dependent thermo-elastic and visco-inertial boundary effects, associated with scattering of ultrasound from the mesoscopic structure of suspensions and dispersions; this is useful for sample characterization in many scientific and industrial applications, especially for particle sizing [4, 214–216].

Resonator-based high-precision sound velocimeters with a resolution of the order of 10^{-6} to 10^{-7} are now available, operating at MHz frequencies in a limited frequency band (typically less than a decade). Because of the increasing absorption at higher frequencies, resonance curves tend to overlap and are therefore less appropriate for high-resolution velocity measurements. At lower frequencies, due to the increasing wavelength, larger sample volumes are necessary, in order to reduce diffraction effects, which broaden resonant peaks. For high resolution excellent temperature stability, without fluctuations and gradients, is mandatory, but it is harder to achieve in larger volumes. For these reasons, relaxation phenomena most often do not fit in the frequency range of one instrument. In addition systems may have several relaxation processes, eventually interfering, leading to a broadband (more than a decade) dispersion characteristic. For such cases precise, broadband sound velocity measurements are indispensable. Outside the presently favoured MHz frequency range, such measurements have to be performed with less accurate techniques. Since the dispersion is normally rather small, e.g. $\Delta c/c < 5 \times 10^{-3}$ for the aqueous system in figure 1, sonic absorption instead of sound velocity spectrometry is often used for broadband ultrasonic studies [75]. Under advantageous conditions, however, both the frequency-dependent relaxational dispersion and the absorption can be measured (figure 1 and [80, 100, 214]) and yield a valuable consistency check of the data.

5. Conclusions

Sound velocimeters have developed from specialized laboratory instruments to commercially available, simple-to-operate analytical tools. Due to their relative simplicity, sound velocity measurements have become quite popular in many fields of material characterization and process control. High resolution velocimeters, either commercial ones or 'home-made' designs and constructions, today can reach a resolution $\Delta c/c \approx 10^{-7}$. The exceptionally demanding sensitivity is obtained with twin cells and the resonator technique. Actually, the velocity difference $(c_s - c_r)$ for a sample and a reference

liquid is determined (figure 19). Since both sound paths are kept in the same massive block, temperature differences are minute and a resolution $\Delta(c_s - c_r) \approx 0.2$ mm s^{-1} becomes possible. Hence, sound velocimetry provides a superior method for the real-time, nondestructive and most sensitive control and evaluation of material properties. The method benefits from its almost universal applicability, as sample property variations are usually accompanied by volume or compressibility changes. A further advantage is the applicability to optically nontransparent samples.

In basic research, sound velocity difference sometimes gets special attention. In figure 2, the temperature dependence of the sound velocity number $u = (c_s - c_r)/(c_r\hat{C})$ for a phospholipid vesicle suspension near its phase transition is shown; here, c_r denotes the sound velocity of the solvent. The variations in c_s are indicated, of course, with the high sensitivity reached by the difference method. The absolute accuracy of the c_s and, in consequence, of the u data, however, is limited by the accuracy of the reference liquid velocity and of the solute concentration $\hat{C}$. The accuracy of the c_r data is substantially lower than the sensitivity in the difference measurements. The sound velocity in water, being the reference in our example (figure 2), is known with an uncertainty $\Delta c_r = 15$ mm s^{-1} [123], corresponding to an error $\Delta c_r/c_r = 10^{-5}$; the error in the phospholipid concentration is even above $\Delta\hat{C}/\hat{C} = 10^{-3}$. Such errors have to be considered when discussing the c_s or u data, respectively, in terms of physical models. In many practical applications further sources of error, such as incomplete wetting of cell cavity surfaces, may affect the c_s data. Though it appears sometimes difficult to quantify such errors, they are essential for the accuracy of the c_s data, as usually they exceed the possible resolution of these measurements significantly. For a resonator-based dual cell velocimeter, error sources have been discussed comprehensively [7].

At present computer-controlled sound velocity measurement systems allow many experimental investigations and control procedures to be run routinely. However, the evaluation of sound velocity profiles in terms of molecular and microscopic sample properties remains a challenging task, when only single-frequency or narrow-bandwidth data are available. If contributions from relaxation processes are involved, smallband or single-frequency data normally do not permit a clear assignment of velocity (and absorption as well) variations to changes either with respect to relaxation amplitude or with respect to relaxation time. The situation becomes even more complex for systems with several relaxation processes. Doubtful interpretations of narrow-band data may be avoided by a preliminary inspection of sample properties, including broadband ultrasonic spectrometry.

References

[1] Douhéret G, Davis M I, Reis J C R and Blandamer M J 2001 Isentropic compressibilities—experimental origin and the quest for their rigorous estimation in thermodynamically ideal liquid mixtures *ChemPhysChem* **2** 148–61

[2] Pfeiffer H and Heremans K 2005 The sound velocity in ideal mixtures from thermal volume fluctuations *ChemPhysChem* **6** 697–705

[3] Kratky O, Leopold H and Stabinger H 1969 Dichtemessungen an Flüssigkeiten und Gasen auf 10^{-6} g cm^{-3} bei 0,6 cm^3 Präparationsvolumen *Z. Angew. Phys.* **27** 273–7

[4] Povey M J W 1997 *Ultrasonic Techniques for Fluids Characterisation* (San Diego: Academic)

[5] Buckin V and Smyth C 1999 High-resolution ultrasonic resonator measurements for analysis of liquids *Semin. Food Anal.* **4** 113–30

[6] Høgseth E, Hedwig G and Høiland H 2000 Rubidium clock sound velocity meter *Rev. Sci. Instrum.* **71** 4679–80

[7] Lautscham K, Wente F, Schrader W and Kaatze U 2000 High resolution and small volume automatic ultrasonic velocimeter for liquids *Meas. Sci. Technol.* **11** 1432–9

[8] Jäger M, Kaatze U, Kudryashov E, O'Driscoll B and Buckin V 2005 New capabilities of high resolution ultrasonic spectroscopy: titration analysis *Spectroscopy* **20** 20–6

[9] Benedetto G, Gavioso R M, Guiliano Albo P A, Lago S, Madonna Ripa D and Spagnolo R 2005 A microwave-ultrasonic cell for sound speed measurements in liquids *Int. J. Thermophys.* **26** 1651–65

[10] Meyer S, Hindle S A, Sandoz J-P, Gan T H and Hutchins D A 2006 Non-contact evaluation of milk-based products using air-coupled ultrasound *Meas. Sci. Technol.* **17** 1838–46

[11] Meier K and Kabelac S 2006 Speed of sound increment for fluids with pressures up to 100 MPa *Rev. Sci. Instrum.* **77** 123903-1-8

[12] Douhéret G, Davis M I and Høiland H 1999 Speeds of sound and excess volumetric properties of mixtures of water with ethylene glycol monopropyl ether at 298.15 K *J. Mol. Liq.* **80** 1–18

[13] Voleišienė B, Miglinienė and Voleišis A 1999 Ultrasonic study of the ionic association in aqueous solutions of lanthanide salts *J. Acoust. Soc. Am.* **105** 962

[14] Voleišienė B, Miglinienė and Voleišis A 2001 Ultrasonic study of the complexation kinetics of yttrium nitrate solutions *Chemija* **12** 225–30

[15] Cutroni M and Mandanici A 2001 The α-relaxation process in simple glass forming liquid *m*-toluidine: II. The temperature dependence of the mechanical response *J. Chem. Phys.* **114** 7124–9

[16] Schmelzer C E H, Żwirbla W, Rosenfeld E and Linde B B J 2004 Acoustic investigations of pseudo-stable structures in in aqueous solutions of polyethylene glycol *J. Mol. Struct.* **699** 47–51

[17] Bae R J 2004 Ultrasonic velocity and absorption measurements in an aqueous solution of poly (sodium 4-styrenesulfonate) *Macromol. Res.* **12** 559–63

[18] Hanke E, Schulz U and Kaatze U 2007 Structural aspects of poly (ethylene glycol)—water mixtures. Isentropic compressibility study *ChemPhysChem* **8** 553–60

[19] Sarvazyan A P 1991 Ultrasonic velocimetry of biological compounds *Annu. Rev. Biophys. Biophys. Chem.* **20** 321–42

[20] Chalikian T V, Sarvazyan A P and Breslauer K J 1994 Hydration and partial compressibility of biological compounds *Biophys. Chem.* **51** 89–109

[21] Chalikian T V and Breslauer K J 1998 Thermodynamic analysis of biomolecules: a volumetric approach *Curr. Opin. Struct. Biol.* **8** 657–64

[22] Halstenberg S, Heimburg T, Hianik, Kaatze U and Krivanek R 1998 Cholesterol-induced variations in the volume and enthalpy fluctuations of lipid bilayers *Biophys. J.* **75** 264–71

[23] Martínez N, Junquera E and Aicart E 1999 Ultrasonic, density and potentiometric characterisation of the interaction of gentisic and gallic acids with an apolar cavity in aqueous solution *Phys. Chem. Chem. Phys.* **1** 4811–7

[24] Kharakoz D P, Khusainova R S, Gorelov A V and Dawson K A 1999 Stochiometry of dipalmitoylphosphatidyl-choline-DNA interaction in the presence of Ca^{2+}: a temperature-scanning ultrasonic study *FEBS Lett.* **446** 27–9

[25] Lee A and Chalikian T V 2001 Volumetric characterisation of the hydration properties of heterocyclic bases and nucleosides *Biophys. Chem.* **92** 209–27

[26] Pfeiffer H and Heremans K 2002 Apparent sound velocity of lysozyme in aqueous solutions *Chem. Phys. Lett.* **361** 226–30

[27] Taulier N and Chalikian T V 2002 Compressibility of protein transitions *Biochem. Biophys. Acta* **1595** 48–70

[28] Schrader W, Ebel H, Grabitz P, Hanke E, Heimburg T, Hoeckel M, Kahle M, Wente F and Kaatze U 2002 Compressibility of lipid mixtures studied by calorimetry and ultrasonic measurements *J. Phys. Chem.* B **106** 6581–6

[29] Chalikian T V 2003 Volumetric properties of proteins *Ann. Rev. Biophys. Biomol. Struct.* **32** 207–35

[30] Hianik T, Rybár P, Benediktyová Z, Svobodá L and Hermetter A 2003 Effects of oxydation on changes of compressibility of bovin serum albumin *Gen. Physiol. Biophys.* **22** 467–76

[31] Hedwig G R and Høiland H 2005 Thermodynamic properties of peptide solutions.XVIII. Partial molar isentropic compressibilities of Gly-X-Gly tripeptides (X = Tyr, Pro, Gln, Asp and Glu), and GlyLysGly acetate in aqueous solution at 25 °C *J. Sol. Chem.* **34** 1297–310

[32] Sarvazyan A, Tatarinov A and Sarvazyan N 2005 Ultrasonic assessment of tissue hydration status *Ultrasonics* **43** 661–71

[33] Taulier N, Beletskaya I V and Chalikian T V 2005 Compressibility changes accompanying conformational transitions of apomyoglobin *Biopolym.* **39** 218–29

[34] Smirnovas V, Winter R, Funck T and Dzwolak W 2005 Thermodynamic properties underlying the α-helix-to-β-sheet transition, aggregation and amyloidogenesis of polylysine as probed by calorimetry, densimetry and ultrasound velocimetry *J. Phys. Chem.* B **109** 19043–5

[35] Smirnovas V, Winter R, Funck T and Dzwolak W 2006 Protein amyloidogenesis in the context of volume fluctuations: a case study of insulin *ChemPhysChem* **7** 1046–9

[36] Pinfield V J, Dickinson E and Povey M J W 1994 Modeling of concentration profiles and ultrasound velocity profiles in a creaming emulsion: importance of scattering effects *J. Colloid Interf. Sci.* **166** 363–74

[37] Pinfield V J, Povey M J W and Dickinson E 1996 Interpretation of ultrasound velocity creaming profiles *Ultrasonics* **34** 695–8

[38] Mosquera V V, del Rio J M, Attwood D, Garcia M, Jones M N, Prieto G, Suarez M J and Sarmiento F 1998 A study of aggregation behavior of hexyltrimethylammonium bromide in aqueous solution *J. Colloid Interf. Sci.***206** 66–76

[39] Dickinson E, Ma J and Povey M J W 1996 Crystallization kinetics in oil-in-water emulsions containing a mixture of solid and liquid droplets *J. Chem. Soc. Faraday Trans.* **92** 1213–5

[40] Hibbard D J, Robinson B H and Robins M M 1999 Ultrasonic characterisation of colloidal dispersions: detection of flocculation and adsorbed layers *Colloids Surf.* B **23** 359–71

[41] Amararene A, Gindre M, Le Huéron J-Y, Urbach W, Valdez D and Waks M 2000 Adiabatic compressibility of AOT (sodium bis (2-ethylhexyl) sulfosuccinate) reverse micelles: analysis of a simple model based on micellar size and volumetric measurements *Phys. Rev.* E **61** 682–9

[42] Tong J and Povey M J W 2002 Pulse echo comparison method with FSUPER to measure velocity dispersion in *n*-tetradecane in water emulsions *Ultrasonics* **40** 37–41

[43] Galán J J, Del Castillo J L, González-Pérez A, Czapkiewicz J and Rodríguez J R 2003 Density and sound velocity studies of aqueous solutions of tetradecyltrimethylammonium nitrate at different temperatures *J. Sol. Chem.* **32** 919–27

[44] Challis R E, Povey M J W, Mather M L and Holmes A K 2005 Ultrasound techniques for characterizing colloidal dispersions *Rep. Prog. Phys.* **68** 1541–637

[45] Panchal K N, Desai A and Nagar T 2006 Sphere-to-rod transition in cationic micelles: quaternary ammonium halides + phenol + water systems *J. Dispers. Sci. Technol.* **27** 963–70

[46] Povey M J W 2000 Particulate characterisation by ultrasound *Pharma. Sci. Technol. Today* **3** 373–80

[47] Serris E, Perier-Camby L, Thomas G, Desfontaines M and Fantozz G 2002 Acoustic emission of pharmaceutical powders during compaction *Powder Technol.* **128** 269–99

[48] Labeit D, Watanabe K, Witt C, Fujita H, Wu Y, Lahmers S, Funck T, Labeit S and Ganzier H 2003 Calcium-dependent molecular spring elements in the giant protein titin *Proc. Natl Acad. Sci.* **100** 13716–21

[49] Han F, Taulier N and Chalikian T V 2005 Association of the Minor Groove Binding Drug Hoechst 33258 with $d(CGCGAATTCGCG)_2$: volumetric, calorimetric, and spectroscopic characterisations *Biochemistry* **44** 9785–94

[50] Medendorp J and Lodder R A 2006 Acoustic-resonance spectrometry as a process analytical technology for rapid and accurate tablet identification *AAPS Pharm. Sci. Tech.* **7** E1–9

[51] Shah R B, Zidan A S, Funck T, Tawakkul M A, Nguyenpho A and Khan M A 2007 Quality by design: characterization of self-nano-emulsified drug delivery systems (SNEDDs) using ultrasonic resonator technology *Int. J. Pharm.* **341** 189–94

[52] Povey M J W 1995 Ultrasound studies of shelf-life and crystallization *New Physico-Chemical Techniques for the Characterization of Complex Food Systems* ed E Dickinson (London: Blackie Academic and Professional) pp 196–213

[53] Benedito J, Carcel J A, Sanjuan N and Mulet A 2000 Use of ultrasound to assess Cheddar cheese characteristics *Ultrasonics* **38** 727–30

[54] Hindle S, Povey M J W and Smith K 2000 Kinetics of crystallization in *n*-hexdecane and cocoa butter oil-in-water emulsions accounting for droplet collision-mediated nucleation *J. Colloid Interf. Sci.* **232** 370–80

[55] Povey M J W and Lamb J 2001 The elastic properties of foods *Handbook of Elastic Properties of Solids, Liquids and Gases* ed M Levy, H Bass and R Stern (New York: Academic)

[56] Létang C, Piom M, Verdier C and Lefebvre L 2001 Characterization of wheat-flour-water doughs: a new method using ultrasound *Ultrasonics* **39** 133–41

[57] Sigfusson H, Ziegler G R and Coupland J N 2001 Ultrasonic monitoring of unsteady-state cooling of food products *Trans. ASAE* **44** 1235–40

[58] Bakkali F, Moudden A, Faiz B, Amghar A, Maze G, Montero de Espinosa F and Akhnak M 2001 Ultrasonic measurement of milk coagulation time *Meas. Sci. Technol.* **12** 2154–9

[59] Benedito J, Carcel J A, Gonzalez R and Mulet A 2002 Application of low intensity ultrasonics to cheese manufacturing processes *Ultrasonics* **40** 19–23

[60] Zhao B, Basir O A and Mittal G S 2003 Correlation analysis between beverage apparent viscosity and ultrasound velocity *Int. J. Food Prop.* **6** 443–8

[61] Cho B-K and Irudayaraj J M K 2003 Foreign object and internal disorder detection in food materials using noncontact ultrasound imaging *J. Food Sci.* **68** 967–74

[62] Cho B-K and Irudayaraj J M K 2003 A noncontact ultrasound approach for mechanical property determination of cheeses *J. Food Sci.* **68** 2243–7

[63] Buckin V, O'Driscoll B and Smyth C 2003 Ultrasonic spectroscopy for material analysis. Recent advances *Spectrosc. Eur.* **15** 20–5

[64] Lehmann L, Kudryashov E and Buckin V 2004 Ultrasonic monitoring of the gelatinisation of starch *Prog. Colloid Polym. Sci.* **123** 136–40

[65] Ross K A, Pyrak-Nolte L J and Campanella O H 2004 The use of ultrasound and shear oscillatory tests to characterize the effect of mixing time on the rheological properties of dough *Food Res. Int.* **37** 567–77

[66] Lehmann L and Buckin V 2005 Determination of the heat stability profiles of concentrated milk and milk ingredients using high resolution ultrasonic spectroscopy *J. Dairy Sci.* **88** 3121–9

[67] Krasaekoopt W, Bhandari B and Deeth H 2005 Comparison of gelation profile of yoghurts during fermentation measured by rva and ultrasonic spectroscopy *Int. J. Food Prop.* **8** 193–8

[68] Dwyer C, Donelly L and Buckin V 2005 Ultrasonic analysis of rennet-induced pre-gelation and gelation processes in milk *J. Dairy Res.* **72** 303–10

[69] Taifi N, Bakkali F, Faiz B, Moudden A, Maze G and Décultot D 2006 Characterization of the syneresis and the firmness of the milk gel using an ultrasonic technique *Meas. Sci. Technol.* **17** 281–7

[70] Eigen M and De Maeyer L 1963 Relaxation methods *Techniques of Organic Chemistry* vol 8, part 2, ed A Weissberger (New York: Interscience) pp 895–1054

[71] Nozdrev V F 1965 *The Use of Ultrasonics in Molecular Physics* (Oxford: Pergamon)

[72] Blandamer M J 1973 *Introduction to Chemical Ultrasonics* (London: Academic)

[73] Stuehr J E 1986 Ultrasonic methods *Investigations of Rates and Mechanisms of Reactions* ed C F Bernasconi (New York: Wiley) pp 247–303

[74] Strehlow H 1992 *Rapid Reactions in Solutions* (Weinheim: VCH)

[75] Kaatze U, Hushcha T O and Eggers F 2000 Ultrasonic broadband spectrometry of liquids: a research tool in pure and applied chemistry and chemical physics *J. Sol. Chem.* **29** 299–368

[76] Herzfeld G and Litovitz T 1959 *Absorption and Dispersion of Ultrasonic Waves* (New York: Academic)

[77] Bhatia A B 1967 *Ultrasonic Absorption. An Introduction to the Theory of Sound Absorption and Dispersion in Gases, Liquids and Solids* (Oxford: Clarendon)

[78] Matheson A J 1971 *Molecular Acoustics* (London: Wiley-Interscience)

[79] Slutsky L J 1981 Ultrasonic relaxation spectroscopy *Methods of Experimental Physics* vol 19, ed P D Edmonds (New York: Academic) pp 179–235

[80] Schwarz G 1968 Kinetic analysis by chemical relaxation methods *Rev. Mod. Phys.* **40** 206–18

[81] Labhardt A and Schwarz G 1976 A high resolution and low volume ultrasonic resonator method for fast chemical relaxation measurements *Ber. Bunsenges. Phys. Chem.* **80** 83–92

[82] Kronig R de L 1926 On the theory of dispersion of x-rays *J. Opt. Soc. Am.* **12** 547–57

[83] Kramers H A 1929 Die Dispersion und Absorption von Röntgenstrahlen *Phys. Z.* **30** 522–3

[84] O'Driscoll B, Kaatze U, Hanke E, Jäger M and Buckin V 2006 Ultrasonic calorimetry of membranes *Pharm. Technol. Eur.* **18** 1–5

[85] Heimburg T 1998 Mechanical aspects of membrane thermodynamics. Estimation of the mechanical properties of lipid membranes close to the chain melting transition from calorimetry *Biochim. Biophys. Acta* **1415** 147–62

[86] Hiedemann E 1939 *Grundlagen und Ergebnisse der Ultraschallforschung* (Berlin: De Gruyter)

[87] Bergmann L 1954 *Der Ultraschall* 6th edn (Stuttgart: Hirzel) Bergmann L 1957 *Nachtrag zum Literaturverzeichnis* (Stuttgart: Hirzel)

[88] Hueter T and Bolt R H 1955 *Sonics* (New York: Wiley)

[89] Schaaffs W 1963 *Molekularakustik* (Berlin: Springer)

[90] Gooberman G L 1968 *Ultrasonics* (London: English University Press)

[91] Kino G S 1987 *Acoustic Waves: Devices, Imaging, and Analog Signal Processing* (Englewood Cliffs, NJ: Prentice-Hall)

[92] Kuttruff H 1988 *Physik und Technik des Ultraschalls* (Stuttgart: Hirzel)

[93] Trusler J P M 1991 *Physical Acoustics and Metrology of Fluids* (Bristol: Hilger)

[94] Dukhin A S and Goetz P J 2002 *Ultrasound for Characterizing Colloids. Particle Sizing, Zeta Potential, Rheology* (Amsterdam: Elsevier)

[95] Tamm K 1961 Schallabsorption und dispersion in wässrigen Elektrolytlösungen *Handbuch der Physik* vol 11/1 ed S Flügge (Berlin: Springer) pp 202–74

[96] McSkimin H J 1964 Ultrasonic methods for measuring the mechanical properties of liquids and solids *Physical Acoustics* vol 1, part A, ed W P Mason (New York: Academic) pp 271–334

[97] Bolef D I and Miller J G 1971 High-frequency continuous wave ultrasonics *Physical Acoustics* vol 8, ed W P Mason (New York: Academic) pp 95–201

[98] Eggers F and Kaatze U 1996 Broad-band ultrasonic measurement techniques for liquids *Meas. Sci. Technol.* **7** 1–19

[99] Kaatze U, Behrends R and Lautscham K 2001 Acoustic relaxation spectrometers for liquids *Ultrasonics* **39** 393–406

[100] Kaatze U and Wehrmann B 1992 Broadband ultrasonic spectroscopy on aqueous solutions of zinc (II) chloride: I. Kinetics of complexation *Z. Phys. Chem.* **177** 9–26

[101] Cedrone N P and Curran D R 1954 Electronic pulse methods for measuring the velocity of sound in liquids and solids *J. Acoust. Soc. Am.* **26** 963–6

[102] Greenspan M and Tschiegg C E 1957 Sing-around ultrasonic velocimeter for liquids *Rev. Sci. Instrum.* **28** 897–901

[103] Myers A, Mackinnon L and Hoare F E 1959 Modifications to standard pulse techniques for ultrasonic velocity measurements *J. Acoust. Soc. Am.* **31** 161–2

[104] Papadakis E P 1967 Ultrasonic phase velocity by the pulse-echo-overlap method. Incorporating diffraction phase corrections *J. Acoust. Soc. Am.* **42** 1045–51

[105] Papadakis E P 1976 New, compact instrument for pulse-echo-overlap measurements of ultrasonic wave transit times *Rev. Sci. Instrum.* **47** 806–13

[106] Aindow J D and Chivers R C 1982 A narrow-band sing-around ultrasonic velocity measurement system *J. Phys. E: Sci. Instrum.* **15** 1027–30

[107] Rogez D and Bader M 1984 Ultrasonic velocity dispersion in liquids between 3.3 and 330 MHz using high resolution phase measurement technique *J. Acoust. Soc. Am.* **76** 167–72

[108] Ernst S, Marczak W, Manikowski R, Zorçbski E and Zorçbski M 1992 A sing-around apparatus for group velocity measurements in liquids. Testing by standard liquids and discussion of errors *Acoust. Lett.* **15** 123–30

[109] Horváth-Szabó G, Høiland M and Høgseth E 1994 An automated apparatus for ultrasound velocity measurements improving the pulse-echo-overlap method to a precision better than 0.5 ppm in liquids *Rev. Sci. Instrum.* **65** 1644–8

[110] Tardajos G, Gonzales Gaitano G and Montero de Espinosa F 1994 Accurate, sensitive and fully automatic method to measure sound velocity and attenuation *Rev. Sci. Instrum.* **65** 2933–8

[111] Hosoda M, Takagi K, Ogawa H, Nomura H and Sakai K 2005 Rapid and precise measurement system for ultrasonic velocity by pulse correlation method designed for chemical analysis *Japan. J. Appl. Phys.* **44** 3268–71

[112] Crawford F S Jr 1968 *Waves—Berkeley Physics Course* vol 3 (New York: McGraw-Hill)

[113] Carstensen E L 1954 Measurement of dispersion of velocity of sound in liquids *J. Acoust. Soc. Am.* **26** 858–61

[114] Cerf R, Degermann H and Bader M 1970 Measure précise de petites différences de vitesse de propagation des ultrasons dans le liquides par comparaison de phase, à l'aide d'une cellule tubulaire *Acustica* **23** 48–9

[115] Kaatze U, Lautscham K and Brai M 1988 Acoustical absorption spectroscopy of liquids between 0.15 and 3000 MHz: II. Ultrasonic pulse transmission method *J. Phys. E: Sci. Instrum.* **21** 98–103

[116] Kaatze U, Kühnel V, Menzel K and Schwerdtfeger S 1993 Ultrasonic spectroscopy of liquids. Extending the frequency range of the variable sample length pulse technique *Meas. Sci. Technol.* **4** 1257–65

[117] Sachse W and Pao Y-H 1978 On the determination of phase and group velocities of disperse waves in solids *J. Appl. Phys.* **49** 4320–7

[118] Kline R A 1984 Measurement of attenuation and dispersion using an ultrasonic spectroscopy technique *J. Acoust. Soc. Am.* **76** 167–72

[119] Goodenough T I J, Rajendram V S, Meyer S and Prête D 2005 Development of a multi frequency pulse diagnostic ultrasound *Ultrasonics* **43** 165–71

[120] Forgacs R L 1960 Improvements in the sing-around technique for ultrasonic velocity measurements *J. Acoust. Soc. Am.* **32** 1697–8

[121] Van Venrooij G E P M 1971 Measurement of ultrasound velocity in human tissue *Ultrasonics* **9** 240–2

[122] Papadakis E P 1973 The measurement of small changes in ultrasonic velocity and attenuation *Crit. Rev. Solid State Sci.* **3** 373–418

[123] Bilaniuk N and Wong S K 1993 Speed of sound in pure water as a function of temperature *J. Acoust. Soc. Am.* **93** 1608–12

[124] McSkimin H J 1961 Pulse superposition method for measuring ultrasonic wave velocities in solids *J. Acoust. Soc. Am.* **33** 12–6

[125] Mitaku S and Sakanishi A 1997 Differential ultrasonic velocimeter for measurements of dilute suspensions *Rev. Sci. Instrum.* **48** 647–50

[126] McClements D J and Fairly P 1991 Ultrasonic pulse echo reflectometer *Ultrasonics* **29** 58–62

[127] Elias M and Garcia-Moliner F 1968 Wave packet propagation and frequency dependent internal friction *Physical Acoustics* vol 5, ed W P Mason and R Thurston (Academic: New York) pp 163–219

[128] Pearson D S, Holtermann G, Ellison P, Cremo C and Geeves A 2002 A novel pressure-jump apparatus for the microvolume analysis of protein-ligand and protein-protein interactions: its application to nucleotide binding to skeletal-muscle and smooth-muscle myosin subfragment-1 *Biochem. J.* **366** 643–51

[129] Nölting B 2005 *Protein Folding Kinetics. Biophysical Methods* (Berlin: Springer)

[130] Hubbard J C 1931 The acoustic resonator interferometer: I. The acoustic system and its equivalent electric network *Phys. Rev.* **38** 1011–9

[131] Eggers F 1967/68 Eine Resonatormethode zur Bestimmung von Schall-Geschwindigkeit und Dämpfung an geringen Flüssigkeitsmengen *Acustica* **19** 323–9

[132] Pethrick R A 1972 The swept frequency resonant interferometer: measurement of acoustic dispersion parameters in the low megahertz frequency range *J. Phys. E: Sci. Instrum.* **5** 571–4

[133] Dev S B, Sarkar S and Pethrick R A 1973 Model calculations for the swept frequency acoustic resonator *J. Phys. E: Sci. Instrum.* **6** 139–44

[134] Sarvazyan A P 1982 Development of methods of precise ultrasonic measurements in small volumes of liquids *Ultrasonics* **20** 151–4

[135] Kaatze U, Wehrmann B and Pottel R 1987 Acoustical absorption spectroscopy of liquids between 0.15 and 300 MHz: high resolution ultrasonic resonator method *J. Phys. E: Sci. Instrum.* **20** 1025–30

[136] Eggers F 1992 Ultrasonic velocity and attenuation measurements in liquids with resonators, extending the MHz frequency range *Acustica* **76** 231–40

[137] Nakajima H and Arakawa K 1993 VHF ultrasonic resonator for soft materials *Japan. J. Appl. Phys.* **32** 2213–5

[138] Eggers F 1994 Analysis of phase slope or group delay time in ultrasonic resonators and its application for liquid absorption and velocity measurements *Acustica* **8** 397–405

[139] Eggers F 1997 Model calculations for ultrasonic plate-liquid-plate resonators: peak frequency shift by liquid density and velocity variations *Meas. Sci. Technol.* **8** 643–7

[140] Kononenko V S 2006 Electric impedance and amplitude-frequency response of a one-dimensional ultrasonic liquid-filled resonator with flat piezoelectric plates *Acoust. Phys.* **52** 696–700

[141] Hagen R, Behrends K and Kaatze U 2004 Acoustical properties of aqueous solutions of urea: reference data for the ultrasonic spectrometry of liquids *J. Chem. Eng. Data* **49** 988–91

[142] Iwanowski I and Kaatze U 2007 Dynamic scaling and slowing down in chemical reactions of the critical triethylamine-water system *J. Phys. Chem.* B **111** 1438–42

[143] Breazeale M A, Cantrell J H Jr and Heyman J S 1981 Ultrasonic wave velocity and attenuation measurements *Methods of Experimental Physics.* vol 19, Ultrasonics, ed P D Edmonds (New York: Academic) pp 67–135

[144] Chu B 1991 *Laser Light Scattering* (New York: Academic)

[145] Takagi K and Negishi K 1982 Measurement of ultrasonic velocity and absorption in liquids up to 1.5 GHz by the high resolution Bragg reflection technique *J. Phys. D: Appl. Phys.* **15** 757–65

[146] Montrose C J, Solovyev V A and Litovitz T A 1967 Brillouin Scattering and relaxation in liquids *J. Acoust. Soc. Am.* **43** 117–30

[147] Chiao R Y, Townes C H and Stoicheff B P 1964 Stimulated Brillouin scattering and coherent generation of intense hypersonic waves *Phys. Rev. Lett.* **12** 592–5

[148] Grubbs W T and McPhail R A 1994 High resolution stimulated Brillouin gain spectrometer *Rev. Sci. Instrum.* **65** 34–41

[149] Sonehara T and Tanaka H 1995 Forced Brillouin spectrometry using frequency-tunable continuous lasers *Phys. Rev. Lett.* **75** 4234–7

[150] Kononenko V S 1997 Precise measurements of elastic wave velocity and dispersion in liquids by an ultrasonic resonator with plane piezoelectric plates *Acoust. Phys.* **43** 354–6

[151] Labhardt A 1975 Konstruktion und Berechnung von Zylinderresonatoren zur Schallabsorptions- und Dispersionsmessung chemischer Relaxationsprozesse *Dissertation* Universität Basel, Basel

[152] Eggers F and Funck Th 1975 New acoustic resonator for liquids in the 0.2 to 2 MHz range *J. Acoust. Soc. Am.* **57** 331–3

[153] Eggers F, Funck Th and Richmann K H 1976 High Q ultrasonic liquid resonators with concave transducers *Rev. Sci. Instrum.* **47** 361–7

[154] Choi P K, Naito Y and Tagaki K 1983 New ultrasonic resonator method using optical diffraction for liquids *J. Acoust. Soc. Am.* **74** 1801–4

[155] Bae J-R, Choi P-K and Tagaki K 1986 Properties of plano-concave ultrasonic resonator and application to velocity dispersion measurement *Japan. J. Appl. Phys.* **25** 1323–6

[156] Eggers F and Richmann K H 1994 Einfache Ultaschall-Resonatoren zur Messung von Dämpfung und Geschwindigkeit unter 100 kHz in Milliliter-Flüssigkeitsproben *Fortschritte der Akustik-DAGA '94* (Bad Honnef: DPG) pp 913–6

[157] Eggers F, Kaatze U, Richmann K H and Telgmann T 1994 New plano-concave ultrasonic resonator cells for absorption and velocity measurements in liquids below 1 MHz *Meas. Sci. Technol.* **5** 1131–8

[158] Behrends R, Eggers F, Kaatze U and Telgmann T 1996 Ultrasonic spectrometry of liquids below 1 MHz. Biconcave resonator cell with adjustable radius of curvature *Ultrasonics* **34** 59–67

[159] Polacek R and Kaatze U 2003 A high-Q easy-to-handle biconcave resonator for acoustic spectrometry of liquids *Meas. Sci. Technol.* **14** 1068–74

[160] Polacek R 2003 Breitbandige Ultraschallabsorptionsspektroskopie an wässrigen ionischen Tensid-Lösungen im Frequenzbereich von 100 kHz bis 2 GHz *Dissertation* Georg-August-Universität, Göttingen

[161] Buckin V, de Maeyer L and Funck T 1994 Ultraschallmeßgerät mit mindestens einem nicht-piezoelektrischen Resonatorkammerkörper und außen angeordneten elektro-akustischen Wandlern *German Patent* DE4313216A1, Bundesdruckerei

[162] Sarvazyan A P, Sel'kov E E and Chalikyan T V 1988 Constant-path acoustic interferometer with transition layers for precision measurements in small liquid volumes *Sov. Phys. Acoust.* **34** 631–4

[163] Sarvazyan A P and Chalikian T V 1991 Theoretical analysis of an ultrasonic interferometer for precise measurements at high pressures *Ultrasonics* **29** 119–24

[164] Sugarawa S 2002 Time difference measurement of ultrasonic pulses using cross-correlation function between analytic signals *Japan. J. Appl. Phys.* **41** 3299–307

[165] McClements D J and Fairley P 1992 Frequency scanning ultrasonic pulse echo reflectometer *Ultrasonics* **30** 403–5

[166] Nelson P V, Povey M J W and Wang Y 2001 An ultrasound velocity and attenuation scanner for viewing the temporal evolution of a dispersed phase in fluids *Rev. Sci. Instrum.* **72** 4234–41

[167] Povey M J W 2001 Ultrasound spectroscopy: the power to transform manufacturing, diagnostics and formulation *Pharm. Visions* **1** 24–8

[168] Loheider S, Vögler G, Petscherizin I, Soltwisch M and Quittmann D 1990 Brillouin scattering on the glass former $GeSBr_2$ *J. Chem. Phys.* **93** 5436–47

[169] Musso M, Aliotta F, Vari C, Aschauer R, Asenbaum A and Wilhelm E 2004 Brillouin scattering in liquid sulfur dioxide relaxation behaviour *J. Mol. Liq.* **110** 33–41

[170] Asenbaum A, Aschauer R, Theisen C, Fritsch T and Wilhelm E 2007 Brillouin scattering in liquid sulfur dioxide *J. Mol. Liquids* **134** 55–7

[171] Ratanaphruks K, Grubbs W T and MacPhail R A 1991 CW stimulated Brillouin gain spectroscopy of liquids *Chem. Phys. Lett.* **182** 371–8

[172] Faris G W, Gerken M, Jirauschek C, Hogan D and Chen Y 2001 High-spectral-resolution stimulated Rayleigh–Brillouin scattering at 1μm *Opt. Lett.* **26** 1894–6

[173] Tanaka H, Sonehara T and Takagi S 1997 A new phase-coherent light scattering method: first observation of complex Brillouin spectra *Phys. Rev. Lett.* **79** 881–4

[174] Tanaka H and Sonehara T 1995 New method of superheterodyne light beating spectroscopy for Brillouin scattering using frequency-tunable lasers *Phys. Rev. Lett.* **74** 1609–12

[175] Hagen R 2003 Breitbandige Ultraschallabsorptionsspektroskopie an wässrigen Kohlehydrat-Lösungen *Dissertation* Georg-August-Universität, Göttingen

[176] Kaatze U, Kühnel V and Weiss G 1996 Variable pathlength cells for precise hypersonic spectrometry of liquids up to 5 GHz *Ultrasonics* **34** 51–8

[177] Pires P F and Guedes H J R 1999 The speed of sound and isentropic compressibility of liquid difluoromethane (HFC32) from $T = (248$ to $343)$ K and pressures up to 65 MPa *J. Chem. Thermodyn.* **31** 55–69

[178] Ball S J and Trusler J P M 2001 Speed of sound of n-hexane and n-hexadecane at temperatures between 298 and 373 K and pressures up to 100 MPa *Int. J. Thermophys.* **22** 427–43

[179] Koski K J, Müller J, Hochheimer H D and Yarger J L 2002 High pressure angle-dispersive Brillouin spectroscopy. A technique for determining acoustic velocities and attenuation in liquids and solids *Rev. Sci. Instrum.* **73** 1235–41

[180] Zhao B, Basir O A and Mittal G S 2005 Estimation of ultrasound attenuation and dispersion using short time Fourier transform *Ultrasonics* **43** 375–81

[181] Kažys R and Čeplys G 2000 Application of wavelet transforms for enhancement of B-type ultrasonic images *Ultragarsas* **35** 21–6

[182] Perov D V and Rinkevich A B 2002 Dyadic-wavelet-transform filtering of ultrasonic signals detected by laser interferometer *Russ. J. Nondestr. Test.* **38** 288–305

[183] Kim Y S and Ra J B 2005 Improvement of ultrasound image based on wavelet transform: speckle reduction and edge enhancement *Proc. SPIE* **5747** 1085–92

[184] Pardo E, San Emetario J L, Rodriguez M A and Ramos A 2006 Noise reduction in ultrasonic NDT using undecimated wavelet transforms *Ultrasonics* **44** (Suppl 1) e1063–7

[185] Truchetet F and Lagliant O 2008 A review on industrial applications of wavelet and multiresolution based signal-image processing *J. Electron. Imaging* at press

[186] Kaur L, Chauhan R C and Saxena S C 2006 Adaptive compression of medical ultrasound images *IEE Proc., Vis. Image Signal Process.* **153** 185–90

[187] Kaur L, Gupta S, Chauhan R C and Saxena S C 2006 Medical ultrasound image compression using joint optimisation of thresholding quantization and best basis selection of wavelet packets *Digit. Sign. Process.* **17** 189–98

[188] Wang P, Shen Y and Wang Q 2007 Gaussian wavelet based dynamic filtering (GWDF) method for medical ultrasound systems *Ultrasonics* **46** 168–76

[189] Zhang Y, Sankar R and Quian W 2007 Boundary delineation in transrectal ultrasound image for prostate cancer *Comp. Biol. Med.* **37** 1591–9
[190] Dencks S, Barkmann R, Padilla F, Haiat G, Laugier P and Glüer C-C 2007 Wavelet-based signal processing of *in vitro* ultrasonic measurements at the proximal femur *Ultrasound Med. Biol.* **33** 970–80
[191] Jhang K, Park B, Jang H and Green R E Jr 2001 Deconvolution of scanning acoustic microscope ultrasonic signals using wavelet transforms to inspect semiconductor die bonds *AIP Conf. Proc.* **557** 571–8
[192] Moholkar V S, Huitema M, Rekveld S and Warmoeskerken M M C G 2002 Characterization of an ultrasonic system using wavelet transforms *Chem. Eng. Sci.* **57** 617–29
[193] Le Goinidec Y and Gibert D 2007 Multiscale analysis of waves reflected by granular media: acoustic experiments on glass beads and effective medium theories *J. Geophys, Res.* **112** B05103–1–12
[194] Rinkevich A B and Perov D V 2005 A wavelet analysis of acoustic fields and signals in ultrasonic non-destructive testing *Russ. J. Nondestruct. Test.* **41** 93–101
[195] Xianfeng F, Zuo M J and Xiaodong W 2006 Identification of weak ultrasonic signals in testing of metallic materials using wavelet transform *Smart Mater. Struc.* **15** 1531–9
[196] Herrera R H, Orozco R and Rodriguez M 2006 Wavelet-based deconvolution of ultrasonic signals in non-destructive evaluation *J. Zhejiang Univ. Sci.* A **7** 1748–56
[197] Tsui P P C and Basir O A 2006 Wavelet basis selection and feature extraction for shift invariant ultrasound foreign body classification *Ultrasonics* **45** 1–14
[198] Honarvar F, Sheikhzadeh H, Moles M and Sinclair A N 2004 Improving the time-resolution and signal-to-noise ratio of ultrasonic NDE signals *Ultrasonics* **41** 755–63
[199] Liang W and Que P-W 2007 Maximum non-Gaussianity parameters estimation of ultrasonic echoes and its application in ultrasonic non-destructive evaluation *Meas. Sci. Technol* **18** 3743–50
[200] Lee S, Pyrak-Nolte L J, Cornillon P and Campanella O 2004 Characterization of frozen orange juice by ultrasound and wavelet analysis *J. Sci. Food Agric.* **84** 405–10
[201] Becker T, Mitzscherling M and Delgado A 2002 Hybrid data model for the improvement of an ultrasonic-based gravity measurement system *Food Control* **13** 223–33
[202] Haller J and Kaatze U 2008 Cyclic carbohydrate-surfactant association and micelle formation in β-cyclodextrin + *n*-decyltrimethylammonium bromide aqueous solutions *Chem. Phys. Lett.* submitted
[203] Wang Q, Bulca S and Kulozik 2007 A comparison of low-intensity ultrasound and oscillating rheology to assess the renneting properties of casein solutions after UHT heat pre-treatment *Int. Dairy J.* **17** 50–8
[204] Elvira L, Durán C, Sierra C, Resa P and Montero de Espinosa F 2007 Ultrasonic measurement device for the characterization of microbiological and biochemical processes in liquid media *Meas. Sci. Technol.* **18** 2189–96
[205] Akasaka K, Latif A R A, Nakamura A, Matsuo K, Tachibana H and Gekko K 2007 Amyloid protofibril is highly voluminous and compressible *Biochem.* **46** 10444–50
[206] Negredo C, Monks E and Sweeney T 2007 A novel real-time ultrasonic method for prion protein detection using plasminogen as capture molecule *BMC Biotechnol.* **7** (43) 1–7
[207] Iwanowski I, Behrends R and Kaatze U 2004 Critical fluctuations near the consolute point of *n*-pentanol-nitromethane. An ultrasonic spectrometry, dynamic light scattering, and shear viscosity study *J. Chem. Phys.* **120** 9192–8
[208] Heimburg T 2007 *Thermal Biophysics of Membranes* (New York: Wiley)
[209] Hickey S, Lawrence M J, Hagan S A and Buckin V 2006 Analysis of the phase diagram and microstructural transitions in phospholipid microemulsion systems using high-resolution ultrasonic spectroscopy *Langmuir* **22** 5575–83
[210] Anisimov M A 1991 *Critical Phenomena in Liquids and Liquid Crystals* (Philadelphia: Gordon and Breach)
[211] Onuki A 2002 *Phase Transition Dynamics* (Cambridge: Cambridge University Press)
[212] Haller J, Behrends R and Kaatze U 2006 Critical fluctuations of the micellar triethylene glycol monoheptyl ether-water system *J. Chem. Phys.* **124** 124910-1-11
[213] Mirzaev S Z, Iwanowski I and Kaatze U 2007 Dynamic scaling and background relaxation in the ultrasonic spectra of the ethanol-dodecane critical mixture *Chem. Phys. Lett.* **435** 263–7
[214] Hipp A K, Storti G and Morbidelli M 1999 Particle sizing in colloidal dispersions by ultrasound. Model calibration and sensitivity analysis *Langmuir* **15** 2338–45
[215] Hibberd D J, Robinson B H and Robins M M 1999 Ultrasonic characterization of colloidal dispersions: detection of flocculation and absorbed layers *Colloid Surf.* B **12** 359–71
[216] Stieler D, Scholle F-D, Weiss A, Ballauff M and Kaatze U 2001 Ultrasonic spectrometry of polystyrene latex suspensions. Scattering and configurational elasticity of polymer chains *Langmuir* **17** 1741–51